Western University

Scholarship@Western

Electronic Thesis and Dissertation Repository

12-9-2014 12:00 AM

Bidentate Ferrocenyl-Dithiol Reagents for Nanocluster Surface Functionalization

Yiyi Liu, *The University of Western Ontario*

Supervisor: Dr. John F. Corrigan, *The University of Western Ontario*
A thesis submitted in partial fulfillment of the requirements for the Master of Science degree in Chemistry

Follow this and additional works at: https://ir.lib.uwo.ca/etd

Part of the Inorganic Chemistry Commons

Recommended Citation

Bidentate Ferrocenyl-Dithiol Reagents for Nanocluster Surface Functionalization

(Thesis format: Monograph)

by

Yiyi <u>Liu</u>

Graduate Program in Chemistry

A thesis submitted in partial fulfillment
of the requirements for the degree of
Master of Science

The School of Graduate and Postdoctoral Studies
The University of Western Ontario
London, Ontario, Canada

© Yiyi Liu 2014

Abstract

Previous work using monodentate ferrocenyl-chalcogen reagents for nanocluster surface functionalization has indicated an effective way to involve ferrocene moieties onto the surface of these frameworks. However, the abilities of the large polynuclear nanocluster with ferrocene rich surface to form crystalline materials suitable for single crystal X-ray analysis proved to be limited. New bidentate ferrocenyl-chalcogen reagents have been synthesized and characterized in order to probe their ability in this case.

The preparation of new bidentate ferrocenyl chalcogen reagents 1,1'-fc(C{O}OCH$_2$CH$_2$SH)$_2$ (fc = ferrocenyl) and 1,1'-fc(C{O}NHCH$_2$CH$_2$SH)$_2$ are presented. Furthermore, the preparation of silylated reagent fc(C{O}OCH$_2$CH$_2$SSiMe$_3$)$_2$ and silver thiolate polymer [fc(C{O}OCH$_2$CH$_2$SAg)$_2$] are discussed. The formation of cluster [Ag$_{74}$S$_{19}$(dppp)$_6$(fc(C{O}OCH$_2$CH$_2$S)$_2$)$_{18}$] using Ph$_2$PCH$_2$CH$_2$CH$_2$PPh$_2$ (dppp) solubilized [fc(C{O}OCH$_2$CH$_2$SAg)$_2$] and the sulfide reagent S(SiMe$_3$)$_2$ as precursors is also described. A single crystal X-ray analysis of [Ag$_{74}$S$_{19}$(dppp)$_6$(fc(C{O}OCH$_2$CH$_2$S)$_2$)$_{18}$] enables a complete description of the molecule, including the arrangement of the ferrocenyl units on the surface.

Cyclic voltammetry and UV-Vis absorption spectroscopy experiments were conducted on the synthesized ligands, complex and clusters, and the results of these experiments are presented.

Keywords

Acknowledgments

I would like to thank all the people who have made this thesis possible. First and foremost, I want to thank my supervisor, Dr. John F. Corrigan, who has enabled the transformation of this 20s year old young into a researcher from a technician, with all his patience, guidance and support. Starting my graduate school in a new country, it was my greatest pleasure to have a supervisor as amazing as John.

I would also like to thank all the chemistry staff for the effort and support they offered to the work presented in this thesis. Firstly, I want to thank our kind glassblower, Yves Rambour: if it is not for his effort to repair all the broken glassware in the lab, I'm sure I would still be struggling there! I'd like to thank the scientists in the NMR facility, Mathew Willans and Aneta Borecki, for their help with the NMR instruments. I want to say "thank you" to the X-ray facility, Paul Boyle and Aneta Borecki, for their support for the X-ray diffractometer. I would also like to thank Doug Hairsine for obtaining all mass spectra for this research, especially for some weird samples that never easily dissolved in anything. All the Chem-Bio Store staff (Marylou Hart, Sherrie McPhee, Don Yakobchuk, Monica Chirigel and Yuhua Chen) is thanked for completing all my requests for chemicals and other supplies. I also want to thank the guys in the Electronics Store, for their help of maintaining the instruments in the lab, especially the two glove boxes. Lastly, I would like to give my thanks to the very helpful Graduate Coordinator, Darlene McDonald, for her help during the two years.

Then I would like to take a moment to say "thank you" to all my colleagues, they are the best lab mates I've met ever! Bahar Khalili Najafabadi and Mahmood Fard are

especially thanked for obtaining all of my X-ray data and solving my structures, also for the guidance at my beginner stage in this lab. I also want to thank my other lab mates, Masoomeh Madadi, Kyle Rozic, Tetyana Levchenko and Alva Zhao. It was all these lab mates who have made my two years here so beautiful and memorable!

I want to thank all my friends back in China and here in Canada for their support. Finally, I would like to give my greatest thanks and appreciation to my family, especially my father and mother. I knew that my parents were the persons who have made all my life real and possible today, if it was not for them I would never be able to stand out here.

Table of Contents

List of Tables

List of Figures

List of Schemes

List of Abbreviations

Å……….Angstrom

^{n}Bu……..n-butyl

^{t}Bu. …….*tert*-butyl

Cp……...cyclopentadineyl

CV…….cyclic voltammetry

dppp……bis(diphenylphosphanyl)propane

E……….chalcogen atom

Et………ethyl

eV……...electron volts

Fc……....CpFe(η^5-C$_5$H$_4$)

fc……….(η^5-C$_5$H$_4$)Fe(η^5-C$_5$H$_4$)

g…..........gram

h………..hours

HRMS….high resolution mass spectroscopy

K……….Kelvin

kJ……….kilojoule

M………..any metal atom

Me……….methyl

MHz…….MegaHertz

mg……….milligram

mL……….milliliter

mmol…….millimole

nm……......nanometer

NMR…….nuclear magnetic spectroscopy

OAc……..acetate

ppm…….parts per million

R………...organic side group

s (NMR)…singlet

THF……...tetrahydrofuran

UV-Vis…ultraviolet-visible

Chapter 1
Introduction: Semiconductor Nanomaterials and the Incorporation of Ferrocene

1.1 Metal Chalcogenide Cluster Chemistry

As an interesting area of research, metal chalcogenide cluster chemistry has been greatly developed during the past 25-30 years and is still drawing the attention of researchers due in part to the size-dependent chemical, physical and structural properties these materials manifest compared to those of the related bulk materials.[1, 2] This class of clusters (and nanoparticles) consist of metal atoms and chalcogens (S, Se, Te) to form the cluster core.[3] Chalcogenide ions E^{2-} (where E is S, Se or Te) can effectively bridge most metals due to the contribution of the large negative charge and large polarizability. HE^-, RE^- and E_x^- (x = 2, 3, 4…) are other members of the family of chalcogen bridging ligands; whereas HE^- is relatively rare while RE^- and E_x^- are more common.[4] The principal reason for the bonding and bridging capacity of these ligands is the negative charge, whereas the uncharged analogues such as E_x, R_2E, REH and H_2E are poorer ligands and rarely form bridging interactions between metal centres. Because the capacity for further bridging, E^{2-} ligands are relatively rare as terminal ligands. Therefore, chalcogenide metal clusters are usually stabilized with additional surface heteroligands, among which chalcogenolate ligands RE^-, halides and phosphines are the biggest three principal classes.[4]

Even with the simple term "metal cluster", there has always been some debate surrounding its definition since the expression was coined by Cotton in the 1960's.[5] According to Cotton, to be considered a metal cluster, the system requires a framework supported "significantly" by metal-metal interactions;[5] this results in the exclusion of those compounds whose framework exists as a result of bridging interactions of non-metallic atoms. This has lead to disagreements, especially in the case of closed shell configuration (d^{10}) metals in which metal-metal bonds are very weak or even nonexistent. Additionally, as far as "cluster" pertains to inorganic chemistry, it also has been used to define semiconductor particles in the nanochemistry field, where the distinctions between molecular clusters, colloids and nanoparticles are also not very clear and the terms are

used rather interchangeably. In this thesis, "cluster" will refer to polynuclear complexes for which the precise structure can be determined by single crystal X-ray crystallography while "nanoparticle" refers to those materials whose precise structure has not been determined.

1.2 Semiconductor Nanomaterials and the Quantum Confinement Effect

A semiconductor can be either a crystalline or amorphous material, but in this case its electrical conductivity will be smaller than that of metals and larger than that of insulators. The conductivity should also be able to be altered by increasing the temperature or the concentration of the impurities (dopants) or by illumination with light due to the increase in the number of charge carriers in the conduction/valence bonds.[6] In the field of nanotechnology, nanomaterials refer to materials that have at least one dimension in the size range 1-100 nm. This class of materials contains a wide range of compounds, including both individual nanostructures, such as clusters, nanoparticles, quantum dots and nanotubes, and the collections and arrays of these structures, for example, as thin films.[7] Semiconductor nanomaterials receive much attention from researchers around the world because of their unique size-dependent optical and electronic properties, which lie between those of the related bulk materials and the related molecular complexes.[1]

Figure 1.1 lays out a schematic representation of the general electronic structure of bulk semiconductors (left), nanometer-sized clusters and colloids (middle), and molecular complexes (right). Bulk semiconductors possess energy bands formed due to the overlapping of the component atomic orbitals, ultimately resulting in the formation of a forbidden bandgap between the filled valence band and the empty conduction band. When an electron is excited into the conduction band, it becomes delocalized and also leaves a delocalized positive charged hole in the valence band. The free particles are delocalized over such a large distance when compared with the lattice constant, thus the electronic properties are independent from the size of the bulk materials. On the opposite

extreme is a molecule, where the linear combination of atomic orbitals leads to the formation of the localized molecular orbitals. Considering intermolecular interactions are weak when compared to intramolecular bonding forces, the electronic properties are generally the sum of the contribution of every single individual and should also be free from their size.[8]
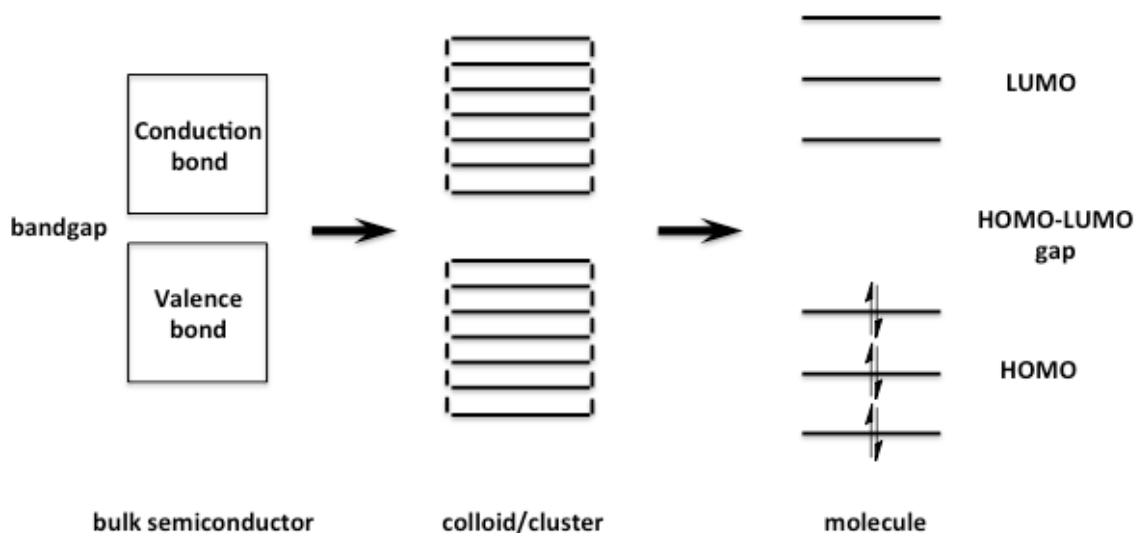
Figure 1.1 Schematic representation of the electronic structure of bulk semiconductors (left), nanometer-sized clusters and colloids (middle), and molecular complexes (right).[1]

However, when the size of the semiconductor material is decreased into the nanometer regime, the situation arises where the size of the particle becomes on the order of, or even smaller than, the wavelength of the propagating electron-hole pairs (also known as Mott-Wannier excitons[9]). Considering the exciton itself as an "atomic species" with a specific Bohr radius, when the size of the nanoparticle decreases smaller than the exciton Bohr radius, the electron-hole pair has to fit in such a small particle with a higher kinetic energy; it is still mobile as in the bulk state, but at the same time also confined to the boundaries of the particle because the Coulombic attraction is not negligible. This is known as the quantum confinement effect.[10, 11, 12] As a result of this confinement, the band gap energy is increased and the energy levels are no longer present as a continuum

near the Fermi level. To a first approximation, the increase in band gap energy, ΔE, is inversely proportional to R^2 (R = the radius of the nanoparticle) as shown by the works by Efros,[13] Brus[14, 15, 16] and Kayanuma,[17, 18] (Eq. 1.1). Their methodology gives out a reasonable estimation of the bandgap for several semiconductor nanoparticles[19, 20, 21, 22] However, comparison with experimental results with theoretic prediction indicates that this model only works perfect with the relatively large particles and breaks down with the smaller ones (<2 nm).

$$\Delta E \ \propto \ \frac{1}{R^2} + \text{other terms} \tag{1.1}$$

1.3 Synthesis of Metal Chalcogenide Clusters and Nanoparticles

Metal chalcogenide clusters, which consist of metal and chalcogen atoms and surface ligands, can in principle be prepared by a large variety of reactions. In general, the synthesis strategy for accessing metal chalcogenide clusters and nanoparticles can be summarized into two methodologies: top down and bottom up, where top-down syntheses start from breaking down bulk materials into smaller species by mechanical, thermal and many other methods while the bottom-up strategies use single atoms or ions to grow clusters and nanoparticles fundamentally.[3]

To make the discussion more detailed, the reactions can be summarized into the following classifications (below). Note that in these examples the inert (non participating) counter cations and counter anions in the unbalanced equations are omitted for clarity.[4]

1. Associations of Ions

$$xM^{n+} + yE^{2-}(or\ HE^- or\ H_2E) \rightarrow [M_xE_y]^z \tag{1.2}$$

$$xM^{n+} + yE^{2-}(or\ HE^- or\ H_2E) + wL \rightarrow [M_xE_yL_w]^z \tag{1.3}$$
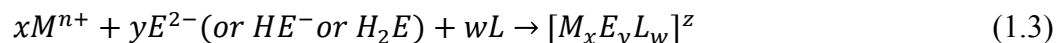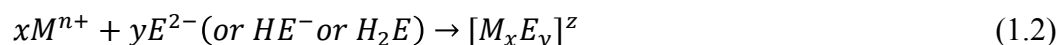
Eq. 1.2 shows the simplest assembly of metal cations and chalcogenide anions, while Eq. 1.3 shows the conditions with the addition of stabilizing heteroligands (L). (M = metal, L = ligand, E = S, Se or Te).

Reactions as in Eq. 1.2 typically generate insoluble, nonmolecular metal chalcogenides instead of molecular clusters, due to the high lattice energies of the uncharged nonmolecular compounds while reactions such as those in Eq. 1.3 can generate soluble species. However, there are still several ways in which these syntheses can be controlled. The first way is utilizing the properties of different solvent systems. Aprotic solvents can usually activate anions by many orders of magnitude rather than protic solvents.[23, 24] For example, the thermodynamic activity of the chloride ion in acetonitrile is almost 10^9 times greater than that in water.[23, 24] The solvent activation of smaller anions can influence reactions as shown in Eq. 1.4, finally establishing an equilibrium between the insoluble (nonmolecular) metal chalcogenide and the soluble molecular species.

$$_\infty[M_a E_b] + E^{2-} \leftrightarrow [M_x E_y]^z \qquad (1.4)$$

A second way to limit the growth of clusters formed by ion association is a physical method. For example, Steigerwald *et al.* used structured micelles in heptane stabilized with the surfactant di(2-ethylhexyl)sulfosuccinate to limit the growth of CdSe.[25] The third method is by applying terminating ligands, where the growth of metal chalcogenide clusters can be limited by the presence of the ligands on their surface.

2. Direct Reaction of the Elements

$$xM + yE \rightarrow [M_x E_y] \qquad (1.5)$$

$$xM + yE + wL \rightarrow [M_x E_y L_w] \qquad (1.6)$$

Shown in Eq. 1.5, cluster formation by direct reaction of the elements is usually acheived by heating a mixture of the bulk material, sometimes with a transfer agent or flux needed for the crystallization of a homogeneous product.[26, 27] This high temperature methodology

normally works well for nonmolecular metal chalcogenides with no surface ligands, while the presence of molecular clusters is less common. However, Rauchfuss and co-workers[28] successfully reacted sulfur with metals in Lewis base solvents at low temperature, forming $Cu_2(S_5)_2L_4$ (following Eq. 1.6), which suggests that under some mild conditions the formation of molecular species with surface ligands is possible via this strategy.

3. Reduction of Chalcogen with Metal Chalcogenolate

$$M(E'R)_n + E \rightarrow [M_xE_y(E'R)_w] + RE'E'R \qquad (1.7)$$

Coordinated or uncoordinated thiolates have the capacity to reduce both elemental sulfur and selenium, but not tellurium[29] (Eq. 1.7). Christou[30] *et al.* originally discovered this synthetic reaction during the formation of $[Se_4Fe_4(SPh)_4]^{2-}$ by reacting a $FeCl_3$-LiSPh mixture with elemental selenium. Elemental sulfur[31] was subsequently used successfully, and this synthetic strategy was developed fully for the synthesis of iron sulfide thiolate complexes.[32, 33]

4. Reaction of a Metal Atom Precursor with a Chalcogen Atom Precursor

$$x''M'' + y''E'' + wL \rightarrow [M_xE_yL_w] \qquad (1.8)$$

This synthetic route (Eq. 1.8) was developed by Steigerwald and co-workers.[34] Considering that phosphine tellurides (such as Et_3PTe) can dissociate to yield elemental Te while Ni(1,5-cyclooctadiene)$_2$ can be used to deliver Ni, by mixing these reagents together intermediate NiTe clusters are then expected. This strategy was shown to be successful upon the formation of $Ni_9Te_6(PEt_3)_8$ and $Ni_{20}Te_{18}(PEt_3)_{12}$.[34] $Pd_6Te_6(PEt_3)_8$ can also be produced by using a soluble source of Pd(0).[35]

5. Elimination of Me₃SiX

$$xMX_n + y(R_3Si)_2E + wL \rightarrow [M_xE_yL_w] + xnR_3SiX \tag{1.9}$$
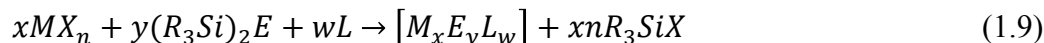
This synthesis strategy is based on the elimination of R₃SiX from the reaction of (R₃Si)₂E[36] with a correlated metal precursor (Eq. 1.9). (R₃Si)₂E is freely soluble in many common solvents (even at low temperature) and the byproducts R₃SiX do not interfere the crystallization process of the clusters. By applying this methodology to phosphine halide complexes of Ni, Co, Cu and Ag (such as [MCl₂(PR₃)₂] (M = Hg) and [MCl(PR₃)] (M = Cu, Ag, Au)), Fenske *et al.*[37] have prepared numerous chalcogen clusters. These impressive frameworks also include the largest metal chalcogenide clusters that could be characterized by single crystal X-ray diffraction so far. The properties of the tertiary phosphine, including its solubility, are a key point of the successful processing and control of this type of reaction. This is shown by the fact that only amorphous, nonmolecular metal sulfides are formed by reacting (Me₃Si)₂S with anhydrous metal halides in CH₂Cl₂, MeCN, or THF without the terminating PR₃ ligands.[38]

6. E-C Scission Reactions

$$[M_m(E'R)_r]^{z-} \rightarrow [M_mE'_s(E'R)_w]^{z-} \rightarrow [M_x(E')_y] \tag{1.10}$$
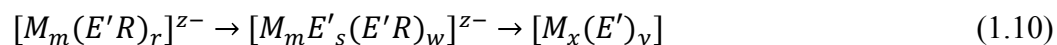
In this type of reaction, organic fragments are eliminated from metal chalcogenolates while metal chalcogenide bonds are formed (Eq. 1.10). Examples of this class of reaction include when excess of NaSMe is treated with NiCl₂ in acetonitrile over a few days, [Ni₃S(SMe)₆]²⁻ is yielded as a result of S-C scission[39]; similarly, excess of NaS*t*-Bu and NiCl₂ in MeOH after a few days yields [Ni₈S(S*t*-Bu)₉]⁻.[40] One important aspect for this type of reaction is that the C-S bond energy of the alkylthiolates is 13-20 kcal mol⁻¹ weaker than that of the arylthiolates, and this is consistent with the evidence that the former is more prevalent when it comes to the formation of metal sulfide clusters by S-C bond scission.[41]

7. Reactions of Silver Thiolate Coordination Polymer with E(SiMe₃)₂

$$xAgSR + yE(SiMe_3)_2 + wL \rightarrow Ag_xE_yL_w + xRSSiMe_3 \qquad (1.11)$$
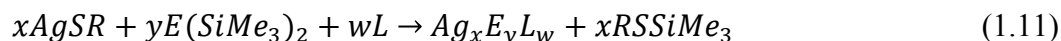
Recently, the synthesis of silver chalcogenate clusters has been reported by using silver thiolate polymer precursors, treating with silylated reagents $E(SiMe_3)_2$ (E = S, Se) and phosphine ligands (Eq. 1.11). Fenske and coworkers have synthesized $Ag_{344}S_{124}(StBu)_{96}$ by using AgStBu and $S(SiMe_3)_2$ and dppxy[42] (dppxy = 1,4-bis(diphenylphosphinomethyl)benzene) and $Ag_{320}(StBu)_{60}S_{130}(dppp)_{12}$ by using AgStBu and $S(SiMe_3)_2$ and dppp (dppp = 1,3-bis(diphenylphosphanyl)propane).[43] The tunability of the R group in the silver thiolate polymer and the ligands has inspired researchers with new synthetic route to the large silver chalcogenate clusters.

1.4 Ag₂S Semiconductor Nanomaterials

In the category of large semiconductor molecules, Ag_2S core based species are now well developed,[44, 45, 46] and attracting more attention since the successful incorporation of sulfide ligands into a preformed $Ag_x(SR)_x$ to yield a nanometer-sized cluster complex.[47] The cluster $[Ag_{50}S_7(SC_6H_4tBu-4)_{40}]^{4-}$ was a first example, isolated from the addition of CS_2 to solutions of a silver 4-tertbutylarylthiolate polynuclear complex. Followed by this report, many other silver sulfide clusters such as $[Ag_{70}S_{16}(SPh)_{34}\bullet(PhCO_2)_4(triphos)_4]$ (triphos = 1,1,1-tris{(disphenylphosphino)methyl}ethane) and $[Ag_{188}S_{94}(PR_3)_{30}]$ have been described.[48] The spherical nature of most of these clusters does not reflect the structure relationship with the bulk Ag_2S material.[49] Even with a large increase in the number of metal atoms, the conversion to a layer-type arrangement of silver and sulfide atoms that would mimic that in the bulk material is still not observed with the largest characterized silver sulfide cluster reported to date, $[Ag_{490}S_{188}(SC_5H_{11})_{114}]$ which displays a double-ellipsoid core structure.[43] (Figure 1.2)

1 nm
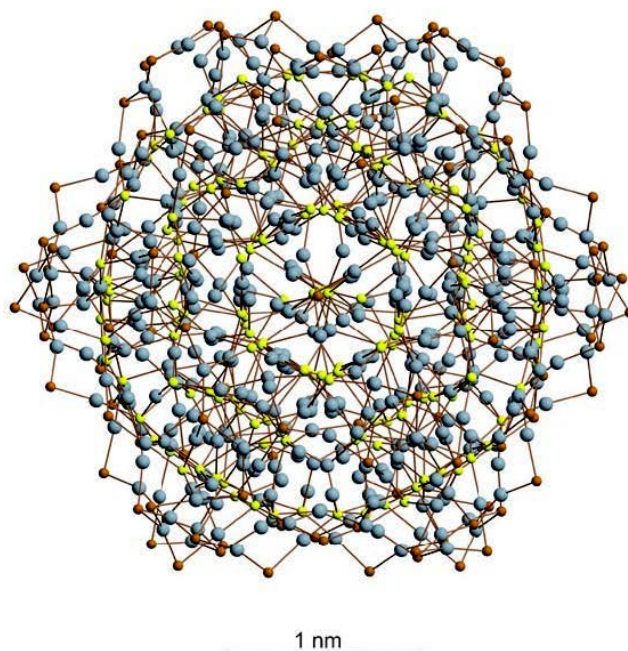
Figure 1.2 Structure of $[Ag_{490}S_{188}(SC_5H_{11})_{114}]$ (C atoms of the C_5H_{11} groups omitted). Ag grey, S in $SC_5H_{11}^-$ orange, S^{2-} yellow.[43]

Large silver-sulfide semiconductor molecules offer advantages when compared to other species of metal chalcogenide clusters, gold nanoparticles and clusters, mainly because of the three primary reasons. Firstly, silver-sulfide is an inexpensive material. Secondly, the oxidation state (I) of silver is quite stable under most conditions, which makes silver sulfide based nanomaterial suitable for many potential electronic applications. For example, ferrocenyl ligands modified silver sulfide cluster only displays one redox curve when processing CV experiments, in which silver atoms are quite stable at the redox potential range of ferrocene and making it the suitable anchor for ferrocenyl ligands.[50] Thirdly and most importantly, compared with other metal chalcogenide materials, which might contain Cd, Hg, Pb, Te and so on, Ag_2S is reported to have negligible toxicity in organisms.[51] Wang and co-workers have further proven this recently by successfully applying a novel near-infrared photoluminescent Ag_2S quantum dots for bioimaging in the living bodies of mice.[52, 53, 54] This has shown that silver sulfide based nanomaterials could be a new bridge between inorganic and biological chemistry.

1.5 A Brief Review of Ferrocene and its Derivatives

Bis(η^5-cyclopentadienyl)iron, most famously known as ferrocene since its accidental discovery in 1951 by Pauson and Kealy[55] and subsequent structure confirmation,[56, 57, 58] helped bring organometallic chemistry to the forefront of chemical research. While several other metallocenes $M(C_5H_5)_2$ (such as $Co(C_5H_5)_2$ and $Ni(C_5H_5)_2$) are often air sensitive and difficult to handle, ferrocene is air stable and can be easily prepared via the reaction of sodium cyclopentadienide with anhydrous ferrous chloride.[59] The metal-ligand interactions within ferrocene involve not only the donation of electron density from the ligand to the metal but also a "back-donation" from the metal to the ligand. Moreover, 12 π electrons in total from two cyclopentadienyl (Cp) rings plus 6 d electrons from Fe^{2+} results in filling the 9 bonding molecular orbitals in ferrocene, thus meeting the requirement of the so-called "18 electron rule".[60] In this way, the stability of ferrocene is not unexpected.

The chemistry of ferrocene is dominant in the field of chemistry for metallocenes, mainly because of its stability and inexpensive commercial availability, which make the preparation of many other ferrocene derivatives and ferrocene containing materials possible. Ferrocene undergoes many reactions that are characteristic of aromatic compounds, enabling the preparation of substituted derivatives, and the substitution can take place at a single site of one Cp ring or multiple sites on both Cp rings. For example, ferrocene can react with *n*-butyl lithium to give 1,1'-dilithioferrocene,[61] while it can also react with *t*-butyl lithium in the presence of *t*-BuOK to give mono lithioferrocene.[62] By applying these lithiation methods, different elements (S, Se, Si, P, N, etc.) and functional groups (carboxylato, amido, phosphido, etc.) can be substituted onto the Cp rings. For example, Beer and coworkers have prepared various ferrocene derivatives,[63, 64, 65] which can be used to selectively detect ions and neutral species.
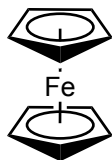
Figure 1.3 Sandwich structure of ferrocene

Figure 1.4 illustrates some of the ferrocene receptors and the species they can selectively detect. These receptors detect specific anions by forming H-bonds between the amide group on the receptor and the anion. The formed receptor-ion pair is more stable than the receptor alone, which can be proven by the comparing the cathodic shifts in oxidation potential upon the addition of the specific anion compared to that of the free receptor when processing the cyclic voltammetric experiments.[66] In this manner the interactions between the ferrocene receptor and anion can be detected electrochemically.

Recently, the synthesis of cluster complexes containing multiple ferrocenyl units has also been attracting much attention because of the optical, electronic and chemical properties these cluster compounds exhibit.[67] These materials can be used as ion sensors and electrode modification materials.[68, 69] Recent efforts have been devoted to the incorporation of multiple ferrocene units into polymers,[70] aromatic,[71] dendrimeric[65, 72] frameworks and inorganic cores.[72, 73, 74, 75] Of these supports, dendrimeric frameworks are the most widely used class due to their large surface-area-to-volume ratio. Dendrimers are nanosized, highly branched molecules which stem from a central core to a periphery, growing bigger with the increasing number of branches. With first examples of ferrocenyl dendrimers appearing in the early 1990's,[76] a variety of these species has been prepared, and the potential usage as electrochemical sensors in the same way mentioned above is being developed. The redox potentials of the ferrocenyl termini are measured by cyclic voltammetry. When a single curve appears, it indicates that all the ferrocene units are oxidized or reduced at the same potential, and thus electronically insulated from each other.[77]
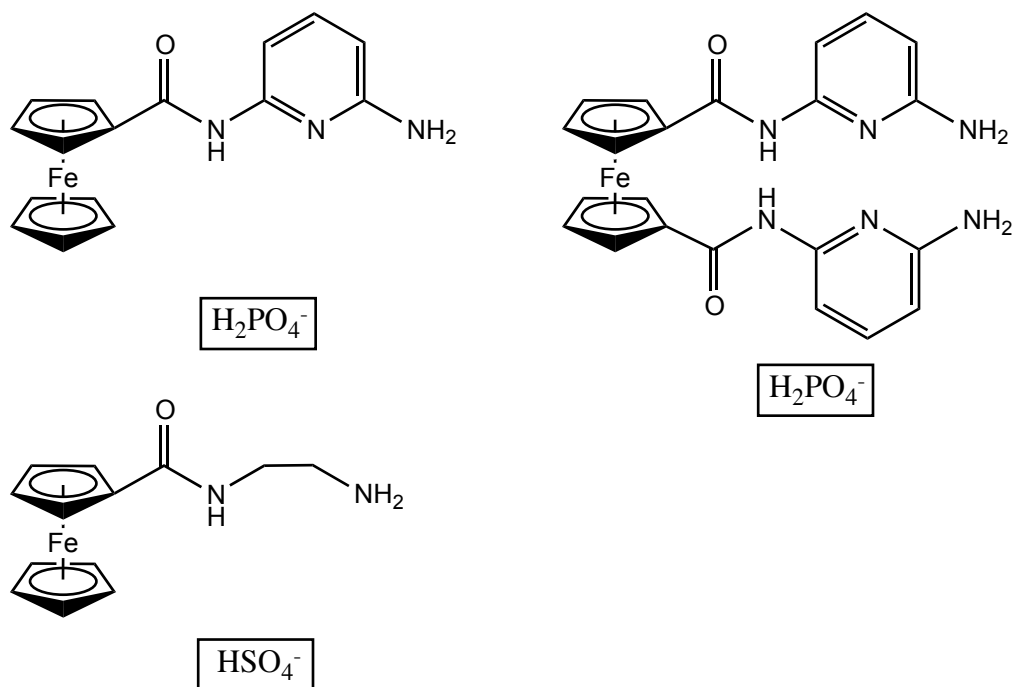
Figure 1.4 Ferrocene based ion sensors and their respective ion detected.[64, 65]

Inorganic cores are another category of material that can be used as support for ferrocene units, among which gold nanoparticles[68, 72] and metal-chalcogenide clusters and nanoparticles[78, 79, 80, 81] are the most common. Numerous examples of ferrocenyl units modified gold nanoparticles have been reported; however, in all of these work the metallic cores are colloid like and never atomically precise, and the redox centers in these materials are spatially removed from the metallic core over time due to the micellar type of stabilization provided by the thiolate ligands.[79] Metal-chalcogenide clusters with ferrocenyl ligands for surface stabilization can yield monodisperse species, whose structures can even be solved by single X-ray diffraction, and thus are attracting more and more attention.

The chemistry of ferrocene is now well understood; however, the potential applications of ferrocene complexes and the related materials still need to be fully discovered. New functionalities and frameworks of ferrocene are to be explored, which could finally lead to novel materials and properties.

1.6 Project Objectives

As discussed earlier, semiconductor nanomaterials possess unique properties, lying between those of the related bulk material and its molecular units. The intrinsic properties of nanomaterials are dependent on the size, and also highly related to the building units that consist of the material.

Recently, the incorporation of ferrocenyl ligands onto the surface of metal chalcogenide clusters has been demonstrated by using $[(\eta^5–C_5H_5)Fe(\eta^5–C_5H_4ESiMe_3)]$ (E = S, Se) precursors, forming the M_4 clusters, $[Cd_4Cl_4\{\mu-(EC_5H_4)Fe(C_5H_5)\}_6]^{2-}$ (E = S, Se),[81, 82] with both clusters having a central core of Cd_4E_6. However, degradation was observed for both of these clusters upon oxidation of the ferrocenyl centers, due to the oxidative cleavage of the ferrocenyl chalcogenate ligands, forming (FcSeSeFc) and (FcSSFc), respectively.

The introduction of a spacer between the metal chalcogen core and the ferrocene unit has been shown successful in avoiding the oxidative cleavage.[72] Due to this, ferrocenyl based ligands containing an alkyl spacer as an insulating bridge between ferrocene and the core, such as $FcCH_2S^-$, $FcC\{O\}OCH_2CH_2E^-$ (E = S, Se) and $FcC\{O\}NHCH_2CH_2E^-$,[50, 83] have been prepared and used for the assembly of redox stable polynuclear complexes with multiple ferrocenyl units such as on the cluster $[Ag_{48}S_6(SCH_2Fc)_{36}]$.[50] These ligands thus show great power in the formation of structurally characterizable metal-chalcogen clusters. However, the clusters synthesized using these ligands are all relatively small clusters, like $[Ag_{48}S_6(SCH_2Fc)_{36}]$ and $[Ag_{14}(PPh_3)_6S(SCH_2CH_2O\{O\}CFc)_{12}]$. Attempts to obtain high-nuclearity clusters with a ferrocene rich surface result in the formation of crystalline materials, such as $[Ag_{36}S_9(SCH_2CH_2O\{O\}CFc)_{18}(PPh_3)_3]$, $[Ag_{100}Se_{17}(SeCH_2CH_2O\{O\}CFc)_{66}(PPh_3)_{10}]$ and $[Ag_{180}Se_{54}(SeCH_2CH_2O\{O\}CFc)_{72}(PPh_3)_{14}$, whose compositions could be formulated on the basis on elemental analysis, high resolution transmission electron microscopy and dynamic light scattering.[84]

The focus of this thesis is to prepare new bidentate ferrocenyl-chalcogen reagents, containing either an ester alkyl group or an amide alkyl group as the insulating bridge between the ferrocene moiety and the chalcogen atom. Bidentate ferrocenyl-chalcogen reagents will have two ligating points when attaching to the surface of clusters, and this may lead to an increased stability/rigidity of the corresponding clusters compared to the ferrocenyl clusters above. The ester functionality was targeted due to its ease of handling while the amide functionality was also developed because it may give the species an oxo-anoin recognition capacity. In this thesis the preparation of two bidentate ferrocenyl-chalcogen reagents are discussed. The ferrocenyl ester dithiol was used for the formation of the nanocluster $[Ag_{74}S_{19}(dppp)_6(fc(C\{O\}OCH_2CH_2S)_2)_{18}]$ (**9**) (dppp = 1, 3-bis(diphenylphosphino)propane). Synthesized compounds were characterized using different methods, such as single crystal X-ray crystallography, NMR spectroscopy, mass spectroscopy, UV-Vis absorption and photoluminescence emission spectroscopy. Cyclic voltammetry studies were carried out for the bidentate ferrocenyl diester ligand (**1**) and the cluster (**9**); ion sensing studies were also performed using $[NBu_4][HSO_4]$.

1.7 References of Chapter 1

1. DeGroot, M. W.; Corrigan, J. F. *Comprehensive Coordination Chemistry II*, eds. McCleverty, J. A.; Meyer, T. J., Elsevier Pergamon, **2004**, *7*.

2. a) Fenske, D. *Clusters and Colloids, From Theory to Applications*; ed. Schmid, G., VCH: Weinheim, **1994**, 212. b) Saito, T. *Early Transition Metal Clusters with π-Donor Ligands*; ed. Chisholm, M. H., VCH: New York, NY, **1995**, 63. c) Dehnen, S.; Eichhöfer, A.; Fenske, D. *Eur. J. Inorg. Chem.* **2002**, 279.

3. Schmid, G.; Fenske, D. *Phil. Trans. R. Soc. A* **2010**, *368*, 1207.

4. Dance, I.; Fisher, K. *Progress in Inorganic Chemistry*, ed. Karlin, K. D., John Wiley & Sons, Inc. **1994**, *41*, 639.

5. Cotton, F. A. Q. *Rev. Chem. Soc.* **1966**, *20*, 389.

6. Papavassiliou, G. C. *Prog. Solid St. Chem.* **1997**, *25*, 126

7. Rao, C. N. R.; Müller, A.; Cheetham, A. K. *The Chemistry of Nanomaterials: Synthesis, Properties and Applications* WILEY-VCH, **2004**, Preface, xvi.

8. Murphy, C. J. *J. Cluster Sci.* **1996**, *7*, 341.

9. a) Wannier, G. K. *Phys. Rev.* **1937**, *52*, 191. b) Mott, N. F. *Trans. Faraday Soc.* **1938**, *34*, 822.

10. Alivisatos, A. P. *Science,* **1996**, *271*, 933.

11. Weller, H. *Angew. Chem. Int. Ed. Engl.* **1993**, *32*, 41.

12. Alivisatos, A. P. *J. Phys. Chem.* **1996**, *100*, 13226.

13. Efros, A. L. *Sov. Phys. Semicond.* **1982**, *16*, 772.

14. Brus, L. E. *J. Chem. Phys.* **1983**, *79*, 5566.

15. Brus, L. E. *J. Chem. Phys.* **1984**, *80*, 4403.

16. Brus, L. E. *J. Chem. Phys.* **1986**, *90*, 2555.

17. Kayanuma, Y. *Solid St. Commun.* **1986**, *59*, 405.

18. Kayanuma, Y. *Phys. Rev. B.* **1988**, *38*, 9797.

19. Nair, S. V.; Sinha, S.; Rustagi, K. C. *Phys. Rev. B.* **1987**, *35*, 4098.

20. Nair, S. V.; Ramaniah, L. M.; Rustagi, K. C. *Phys. Rev. B.* **1992**, *45*, 5969.

21. Norris, D. J.; Bawendi, M. G. *Phys. Rev. B.* **1996**, *53*, 16338.

22. Norris, D. J.; Sacra, A.; Murray, C. B.; Bawendi, M. G. *Phys. Rev. Lett.* **1994**, *72*, 2612.

23. Alexander, R.; Ko, E. C. F.; Parker, A. J.; Broxton, T. J. *J. Am. Chem. Soc.* **1968**, *90*, 5049.

24. Parker, A. J. *Chem. Rev.* **1969**, *69*, 1.

25. Steigerwald, M. L.; Alivisatos, A. P.; Gibson, J. M.; Harris, T. D.; Kortan, R.; Muller, A. J.; Thayer, A. M.; Duncan, T. M.; Douglass, D. C.; Brus, L. E. *J. Am. Chem. Soc.* **1988**, *110*, 3046.

26. Bronger, W. *Angew. Chem. Int. Ed. Engl.* **1981**, *20*, 52.

27. Sunshine, S. A.; Kang, D.; Ibers, J. A. *J. Am. Chem. Soc.* **1987**, *109*, 6202.

28. Ramli, E.; Rauchfuss, T. B.; Stern, C. L. *J. Am. Chem. Soc.* **1990**, *112*, 4043.

29. Lee, G. S. H. Ph. D. thesis, *"Synthesis and Spectroscopic Investigations of Cadmium Chalcogenide Macromolecules",* University of New South Wales, Australia, **1992**.

30. Christou, G.; Ridge, B.; Rydon, N. H. *J. Chem. Soc. Dalton Trans.* **1978**, *10*, 1423.

31. Christou, G.; Garner, C. D. *J. Chem. Soc. Dalton Trans.* **1979**, *6*, 1093.

32. Hagen, K. S.; Reynolds, J. G.; Holm, R. H. *J. Am. Chem. Soc.* **1981**, *103*, 4054.

33. Hagen, K. S.; Holm, R. H. *J. Am. Chem. Soc.* **1982**, *104*, 5496.

34. Brennan, J. G.; Siegrist, T.; Stuczynski, S. M.; Steigerwald, M. L. *J. Am. Chem. Soc.* **1989**, *111*, 9240.

35. Brennan, J. G.; Siegrist, T.; Stuczynski, S. M.; Steigerwald, M. L. *J. Am. Chem. Soc.* **1990**, *112*, 9233.

36. Drake, J. E.; Glavincevski, B. M.; Hemmings, R. T.; Henderson, H. E. *Inorg. Synth.* **1980**, *20*, 171.

37. Fenske, D.; Ohmer, J.; Hachgenei, J.; Nerzweiler, K. *Angew. Chem. Int. Ed. Engl.* **1988**, *27*, 1277.

38. Martin, M. J.; Qiang, G-H.; Schleich, D. M. *Inorg. Chem.* **1988**, *27*, 2804.

39. Henkel, G.; Kriege, M.; Matsumoto, K. *J. Chem. Soc. Dalton Trans.* **1988**, *3*, 657.

40. Kruger, T.; Krebs, B.; Henkel, G. *Angew. Chem. Int. Ed. Engl.* **1989**, *28*, 61.

41. Lee, W-L.; Gage, D. A.; Huang, Z-H.; Chang, C. K.; Kanatzidis, M. G.; Allison, J. *J. Am. Chem. Soc.* **1992**, *114*, 7132.

42. Fenske, D.; Anson, A. E.; Eichhöfer, A.; Fuhr, O.; Ingendoh, A.; Persau, C.; Richert, C. *Angew. Chem. Int. Ed.* **2005**, *44*, 5242.

43. Anson, C.E.; Eichhöfer, A.; Issac, I.; Fenske, D.; Fuhr, O.; Sevillano, P.; Persau, C.; Stalke, D.; Zhang, J. *Angew. Chem. Int. Ed.* **2008**, *47*, 1326.

44. Corrigan, J. F.; DeGroot, M. W. *The Chemistry of Nanomaterials: Synthesis, Properties and Applications*, eds. Rao, C. N. R.; Müller, A.; Cheetham, A. K., WILEY-VCH, **2004**, *2*, 418.

45. Jain, S.; Willander, M.; Van Overstraetan, R. *Compound Semiconductors Strained Layers and Devices*, eds. Willoughby, A. F. W.; Hull, R., Electronic Materials *7*, Kluwer Academic, Boston, **2000**, 214.

46. Janssen, M. D.; Grove, D. M.; Van Koten, G. *Prog. Inorg. Chem.* **1997**, *46*, 97.

47. Tang, K.; Xie, X.; Zhang, Y.; Zhao, X.; Jin, X. *Chem. Commun.* **2002**, 1024.

48. Wang, X.; Langetepe, T.; Persau, C.; Kang, B.; Sheldrick, G. M.; Fenske, D. *Angew. Chem. Int. Ed.* **2002**, *41*, 3818.

49. Dehnen, S.; Eichhöfer, A.; Fenske, D. *Eur. J. Inorg. Chem.* **2002**, 279.

50. Ahmar, S.; MacDonald, D. G.; Vijayaratnam, N.; Battista, T. L.; Workentin, M. S.; Corrigan, J. F. *Angew. Chem. Int. Ed.* **2010**, *49*, 4422.

51. Hirsch, A. P. *Environ. Toxicol. Chem.* **1998**, *17*, 601.

52. Du, Y.; Xu, B.; Fu, T.; Cai, M.; Li, F.; Zhang, Y.; Wang, Q. *J. Am. Chem. Soc.* **2010**, *132*, 1470.

53. Zhang, Y.; Hong, G.; Zhang, Y.; Chen, G.; Li, F.; Dai, H.; Wang, Q. *ACS Nano* **2012**, *6*, 3695.

54. Li, C.; Zhang, Y.; Wang, M.; Zhang, Y.; Chen, G.; Li, L.; Wu, D.; Wang, Q. *Biomater.* **2014**, *35*, 393.

55. Kealy, T. J.; Pauson, P. L. *Nature* **1951**, *4285*, 1039.

56. Eiland, P. F.; Pepinsky, R. *J. Am. Chem. Soc.* **1952**, *19*, 4971.

57. Dunitz, J. D.; Orgel, L. E. *Nature* **1953**, *4342*, 121.

58. Dunitz, J.; Oregl, L.; Rich, A. *Acta Crystallogr.* **1956**, *9*, 373.

59. Wilkinson, G. *Org. Synth.* **1956**, *36*, 31.

60. Beswick, M. A.; Palmer, J. S.; Wright, D. S. *Chem. Soc. Rev.* **1998**, *27*, 225.

61. Roussier, R.; Abdulla, A.; Gautheron, B. *J. Organomet. Chem.* **1987**, *332*, 165.

62. Breti, B.; Breuninger, D. *Synthesis* **2005**, *16*, 2782.

63. Beer, P. D.; Hayes, E. J. *Coord. Chem. Rev.* **2003**, *240*, 167.

64. Beer, P. D. *Chem. Commun.* **1996**, 689.

65. Beer, P. D.; Gale, P. A. *Angew. Chem. Int. Ed.* **2001**, *40*, 486.

66. Beer, P. D.; Bayly, S. R. *Top Curr. Chem.* **2005**, *25*, 125.

67. Togni, A.; Hayashi, T. *Ferrocenes: Homogeneous Catalysis, Organic Synthesis, Materials Science,* VHC, Weinheim, **1994**.

68. Labande, A.; Ruiz, J.; Astruc, D. *J. Am. Chem. Soc.* **2002**, *124*, 1782.

69. Li, M.; Cai, P.; Duan, C.; Lu, F.; Xie, J.; Meng, Q. *Inorg. Chem.* **2004**, *43*, 5174.

70. Nguyen, P.; Elipe, P. G.; Manners, I. *Chem. Rev.* **1999**, *99*, 1515.

71. Nakashima, S.; Nakazaki, S.; Sakai, H.; Watanabe, M.; Motoyama, I.; Sato, M. *Inorg. Chem.* **1998**, *37*, 1959.

72. Astruc, D.; Daniel, M-C.; Ruiz, J. *Chem. Commun.* **2004**, 2637.

73. Adams, R. D.; Qu, B. *J. Organomet. Chem.* **2001**, *620*, 303.

74. Chandrasekhar, V.; Nagendran, S.; Bansal, S.; Kozee, M. A.; Powell, D. R. *Angew. Chem. Int. Ed.* **2000**, *39*, 1833.

75. Nitschke, C.; Wallbank, A. I.; Fenske, D.; Corrigan, J. F. *J. Cluster Sci.* **2007**, *18*, 131.

76. Fillaut, J. L.; Astruc, D. *J. Chem. Soc. Chem. Commun.* **1993**, 1320.

77. Astruc, D. *Electron Transfer and Radical Processes in Transition-Metal Chemistry,* VCH, New York, **1995**.

78. Nitschke, C.; Fenske, D.; Corrigan, J. F. *Inorg. Chem.* **2006**, *45*, 9394.

79. a) Wallbank, A. I.; Corrigan, J. F. *Chem. Commun.* **2001**, 377. b) Wallbank, A. I.; Corrigan, J. F. *J. Cluster Sci.* **2004**, *15*, 225.

80. Lebold, T. P.; Stringle, D. L. B.; Workentin, M. S.; Crooigan, J. F. *Chem. Commun.* **2003**, 1398.

81. a) Chandrasekhar, V.; Nagendran, S.; Bansal, S.; Kozee, M. A.; Powell, D. R. *Angew. Chem. Int. Ed.* **2000**, *39*, 1833. b) Zheng, G. L.; Ma, J. F.; Su, Z. M.; Yan, L. K.; Yang, J.; Li, Y. Y.; Liu, J. F. *Angew. Chem. Int. Ed.* **2004**, *43*, 2409. c) Astruc, D. *Acc. Chem. Res.* **1997**, *30*, 383.

82. Borecki, A. Undergraduate Chemistry 490 Thesis, The University of Western Ontario, **2004**.

83. MacDonald, D. G.; Eichhöfer, A.; Campana, C. F.; Corrigan, J. F. *Chem. Eur. J.* **2011**, *17*, 5890.

84. MacDonald, D. G.; Kübel, C.; Corrigan, J. F. *Inorg. Chem.* **2011**, *50*, 3252.

Chapter 2
Preparation and Characterization of Bidentate Ferrocenyl-Dithiol Reagents

2.1 Introduction

New ferrocenyl derivatives and ferrocene containing compounds are the focus of many researchers.[1, 2] The stability and ease of modification on the cyclopentadienyl rings combined with the fact that ferrocene an inexpensive material, have made it a very good candidate for a source of a redox active center. However, one of the challenges synthetic chemists still face is how to design appropriate ferrocenyl ligands and allow the incorporation of this desired redox center into different frameworks.

Ferrocene containing materials have potential applications in electronic devices including their usage in ion sensing.[3] Although there are numerous ferrocene derivatives reported, examples of well defined nanosized structural frameworks are still rare. Two primary reasons for this situation are: (i) lack of ferrocenyl chalcogenate ligands available for the nanosized assembling; (ii) lack of control over the reaction process to allow the formation of suitable crystals for structural characterization.

Ferrocene can react with *n*-butyl lithium along with *N,N,N',N'*-tetramethylethylenediamine (TMEDA) to give 1,1'-dilithioferrocene,[4] while it reacts with *t*-butyl lithium in the presence of *t*-BuOK to give mono lithioferrocene.[5] By applying different synthetic methods to either dilithioferrocene or lithioferrocene, bidentate or monodentate ferrocene derivatives can be synthesized. For example, by purging CO_2 in solution of lithioferrocene or dilithioferrocene, ferrocene carboxylate or 1,1'-ferrocene dicarboxylate can be synthesized, making the further ester or amide functionalization on ferrocene possible. Some examples of ferrocenyl chalcogenolate ligands reported to date include: 1,1'-Fe(η^5-$C_5H_4ESiMe_3$)$_2$ (E = S, Se) used in the preparation of polynuclear Cu and Ag clusters with multiple ferrocenyl units and monomeric Pd and Pt complexes;[6, 7, 8, 9] CpFe(η^5-$C_5H_4CH_2ESiMe_3$) (E = S, Se) used in the preparation of the [$Ag_{48}S_6(SCH_2Fc)_{36}$] cluster and other silver complexes;[10] CpFe(η^5-

$C_5H_4C\{O\}XCH_2CH_2ESiMe_3$) (X = O, NH; E = S, Se) in the preparation of $[Ag_{14}(PPh_3)_6S(SCH_2CH_2O\{O\}CFc)_{12}]$ cluster and other high-nuclearity ferrocene containing materials.[11] In the following sections, the preparation and characterization of the bidentate ferrocenyl chalcogen reagents 1,1'-fc$(C\{O\}OCH_2CH_2SH)_2$ (**4**), 1,1'-fc$(C\{O\}OCH_2CH_2SSiMe_3)_2$ (**6**), 1,1'-fc$(C\{O\}NHCH_2CH_2SH)_2$ (**8**) and the related silver thiolate coordination polymer fc$(C\{O\}OCH_2CH_2SAg)_2$ (**5**), will be presented.

2.2 Materials and Methods

2.2.1 General Synthetic Techniques and Starting Materials

Because of the air and moisture sensitivity of the reagents and products, all experimental procedures (except for column chromatography) were performed using standard double manifold Schlenk line techniques under a dry and high purity nitrogen atmosphere, or in a MBraun inert atmosphere (N_2) glovebox. Non-chlorinated solvents (THF, diethyl ether, hexanes, pentane and heptane) were dried and collected using an MBraun MB-SP Series solvent purification system with tandem activated alumina (THF, ether), an activated alumina and activated copper redox catalyst (hydrocarbons). The chlorinated solvents (chloroform, deuterated chloroform and dichloromethane) and acetonitrile were dried and distilled over P_2O_5.

1.6 M n-Butyllithium in hexanes (n-BuLi), ferrocene (98%), tetrabutylammonium fluoride (TBAF), oxalyl chloride, 2-chloroethylamine, 1-hydroxybenzotriazole (HoBt) and tetrabutylammonium bisulfate (≥99.0%) were purchased from Aldrich. 1-(3-Dimethylaminopropyl)-3-ethylcarbodiimide hydrochloride (EDC) and silver trifluoromethanesulfonate (98%) were purchased from Alfa Aesar. The silylated reagent $S(SiMe_3)_2$ was prepared according to literature procedures.[12] Triethylamine and *N,N,N',N'*-tetramethylethylenediamine (TMEDA) were distilled and kept under nitrogen atmosphere. Celite was dried by heating at 120 ˚C under vacuum for 48 hours. 1,1'-Ferrocene dicarboxylic acid was prepared according to literature methods.[13]

2.2.2 Characterization

Solution ^{1}H and ^{13}C{^{1}H} NMR spectra were obtained on a Varian Mercury VX 400 MHz spectrometer at operating frequencies of 400.08 and 100.61 MHz, respectively. ^{1}H and ^{13}C{^{1}H} NMR spectra were referenced internally to signals from residual H and to the C atoms, respectively, of the deuterated solvent, relative to tetramethylsilane (TMS) at 0 ppm. Elemental analyses were performed by Laboratoire d'analyse élémentaire, Université de Montréal (Montréal, Canada). High-resolution mass spectrometry was recorded on a Finnigan MAT 8400 mass spectrometer. UV/Vis absorption spectra were recorded on a Varian Cary 300 Bio UV/Vis spectrophotometer.

All single crystal X-ray diffraction measurements were performed on a Bruker APEX-II diffractometer at 150 K or 110 K, with the molecular structures solved via direct methods using the SHELX suite of crystallographic programs (Sheldrick, G. M., Madison, WI).[14]

2.3 Experimental

2.3.1 Synthesis of 1 (1,1'-fc(C{O}OCH$_2$CH$_2$Br)$_2$) , 2 (1,1'-fc(C{O}OCH$_2$CH$_2$Br)COOH) and 3 ((fc(C{O}O{O}C))$_2$)

Oxalyl chloride (1.6 mL, 19 mmol) in 8 mL CH$_2$Cl$_2$ was added slowly to a well-stirred suspension of fc(COOH)$_2$ (1.0 g, 3.7 mmol) in 30 mL CH$_2$Cl$_2$. 20 drops of DMF were given as a catalyst to activate the reaction and the solution was stirred for about 1 hour. The solvent was removed and another 30 mL of CH$_2$Cl$_2$ was added to dissolve the product. The solution was cooled to 0 ˚C and NEt$_3$ (2.3 mL, 16 mmol) and BrCH$_2$CH$_2$OH (1.2 mL, 17 mmol) were added; the mixture was stirred at 0 ˚C for 2 hours and then at RT for another 2 hours. The product was concentrated to ~10 mL and adsorbed onto a minimum amount of silica gel. The silica was dried and a silica column was run, using 1:1 mixture of hexanes and diethyl ether as eluent. Product **1**, **2** and **3** were collected in the order of time, respectively. Yield for **1** = 0.92 g (51%), yield for **2** = 0.36 g (26%), yield for **3** = 0.10 g (10%). Characterization for **1**: ^{1}H NMR (400 MHz, CDCl$_3$, 23 ˚C): δ = 4.89 (m, 4H, CH), 4.54 (t, ^3J = 6.0 Hz, 4H, CH$_2$), 4.48 (m, 4H, CH), 3.65 (t, ^3J = 6.0 Hz,

4H, CH$_2$); ^{13}C{^{1}H} NMR (100.5 MHz, CDCl$_3$): δ = 170.0 (C(O)), 73.2 (CH), 72.1 (C), 71.8 (CH), 63.8 (CH$_2$), 29.2 (CH$_2$); elemental analysis calcd (%) for C$_{16}$H$_{16}$O$_4$Br$_2$Fe: C 39.38, H 3.31; found: C 39.52, H 3.37. Characterization for **2**: ^{1}H NMR (400 MHz, CDCl$_3$, 23 ˚C): δ = 4.89-4.95 (m, 4H, CH), 4.55 (t, ^3J = 6.0 Hz, 2H, CH$_2$), 4.51 (m, 4H, CH), 3.64 (t, ^3J = 6.0 Hz, 2H, CH$_2$); ^{13}C{^{1}H} NMR (100.5 MHz, CDCl$_3$): δ = 176.1 (C(O)O), 169.9 (C(O)), 73.6 (CH), 73.3 (CH), 72.5 (C), 72.4 (C), 72.2 (CH), 72.0 (CH), 63.9 (CH$_2$), 29.0 (CH$_2$); elemental analysis calcd (%) for C$_{14}$H$_{13}$O$_4$BrFe: C 44.14, H 3.44; found C 44.59, H 3.29. Characterization for **3**: ^{1}H NMR (400 MHz, CDCl$_3$, 23 ˚C): δ = 5.06 (m, 8H, CH), 4.68 (m, 8H, CH); ^{13}C{^{1}H} NMR (100.5 MHz, CDCl$_3$): δ = 173.8 (C(O)), 73.9 (CH), 73.8 (C), 73.4 (CH); HRMS: *m/z*: calcd for C$_{24}$H$_{16}$O$_6$Fe$_2$: 511.9646; found: 511.9640; m.p.: decomposed at 184 ˚C -188 ˚C.

2.3.2 Synthesis of 4 (fc(C{O}OCH$_2$CH$_2$SH)$_2$)

1 (0.41 g, 0.84 mmol) was dissolved in THF (25 mL) and the solution was cooled to -10 ˚C. S(SiMe$_3$)$_2$ (0.53 mL, 2.5 mmol), was added, followed by TBAF (0.48 g, 1.8 mmol) in THF (15 mL). The reaction was stirred for 10 min at -10 ˚C and the mixture was subsequently stirred at RT for 3.5 hours. The solvent was removed under vacuum, and 35 mL THF was used to dissolve the residue. 35 ml of heptane was added to the flask and the majority of THF was removed under vacuum. The orange solution was filtered over dry Celite and heptane was removed under vacuum to yield **4** as a dark orange solid. A quick silica column using EtOAc as eluent can be applied according to the purity of the product. Yield = 0.25 g (75%). ^{1}H NMR (400 MHz, CDCl$_3$, 23 ˚C): δ = 4.85 (m, 4H, CH), 4.45 (m, 4H, CH), 4.36 (t, ^3J = 6.4 Hz, 4H, CH$_2$), 2.87 (dt, ^3J = 6.4 Hz, ^2J = 8.0 Hz, 4H, CH$_2$), 1.60 (t, ^3J = 8.0 Hz, 2H, SH); ^{13}C{^{1}H} NMR (100.5 MHz, CDCl$_3$): δ = 169.8 (C(O)), 73.0 (CH), 72.4 (C), 71.7 (CH), 65.7 (CH$_2$), 23.5 (CH$_2$); HRMS: *m/z*: calcd for C$_{16}$H$_{18}$Fe$_1$O$_4$S$_2$: 393.99961; found: 393.99860.

2.3.3 Synthesis of 5 ([fc(C{O}OCH₂CH₂SAg)₂]ₙ)

To a solution of 230 mg (0.59 mmol) of **4** in 20 mL CH_3CN was added a solution of silver triflate (0.38 g in 10 mL CH_3CN, 1.47 mmol), and stirring was maintained for 5 mins. 0.19 mL of NEt_3 (1.35 mmol) was added and an orange precipitate formed. The yellow precipitate was collected via filtration and washed with 4 x 10 mL of CH_3CN. The precipitate was dried under vacuum. Yield = 0.13 g (36%). Elemental analysis calcd (%) for $C_{16}H_{16}O_4S_2Ag_2Fe$: C 31.62, H 2.65, S 10.52; found: C 32.25, H 2.76, S 9.67; m.p.: 173 ˚C -177 ˚C.

2.3.4 Synthesis of 6 (fc(C{O}OCH₂CH₂SSiMe₃)₂)

NEt_3 (0.39 mL, 2.82 mmol) and $ClSiMe_3$ (0.36 mL, 2.82 mmol) were added to a solution of **4** (0.22 g, 0.56 mmol) in 20 mL THF at 0 ˚C. The reaction mixture was stirred at 0 ˚C for 50 min and then at RT for overnight. 20 mL of heptane was added and the majority of THF was removed under vacuum. The orange solution was filtered over dry Celite and washed with 2 x 10 mL dry heptane. Heptane was removed under vacuum to yield **6** as orange oil. Yield = 0.43 g (95%). ^{1}H NMR (400 MHz, $CDCl_3$, 23 ˚C): δ = 4.85 (m, 4H, CH), 4.44 (m, 4H, CH), 4.30 (t, ^3J = 4.8 Hz, 4H, CH_2), 2.81 (t, ^3J = 4.8 Hz, 4H, CH_2), 0.37 (s, 18H, $SiMe_3$); ^{13}C{^{1}H} NMR (100.5 MHz, $CDCl_3$): δ = 170.2 (C(O)), 73.1 (CH), 72.6 (C), 71.7 (CH), 65.2 (CH_2), 24.7 (CH_2), 1.0 ($SiMe_3$); HRMS: *m/z*: calcd for $C_{22}H_{34}O_4FeS_2Si_2$: 538.07867; found: 538.07668.

2.3.5 Synthesis of 7 (fc(C{O}NHCH₂CH₂Cl)₂)

EDC•HCl (1.5 g, 7.7 mmol), $H_2NCH_2CH_2Cl$•HCl (0.85 g, 7.3 mmol), 3.2mL (22 mmol) of NEt_3 and HoBt (0.49 g, 3.6 mmol) were added to a suspension of 1,1'-ferrocene dicarboxylic acid (1.0 g in 50 mL of dichloromethane, 3.7 mmol) at 0 ˚C. The temperature of the reaction was raised to RT gradually and the mixture was stirred for approximately 21 hours. Filtration over dried Celite yielded an orange filtrate, which was washed 3 times with degassed water (3 × 40 mL). The crude product was concentrated to ~ 10 mL and absorbed onto minimum amount of silica gel. The silica was dried and

separation was performed via column chromatography (silica) using EtOAc: hexanes (3: 1) as eluent. Yield = 0.62 g (43%). ^{1}H NMR (400 MHz, CDCl$_3$, 23 ˚C): δ = 7.04 (s, 2H, NH), 4.57 (m, 4H, CH), 4.42 (m, 4H, CH), 3.76 (m, 8H, 2CH$_2$); ^{13}C{^{1}H} NMR (100.5 MHz, CDCl$_3$): δ = 170.7 (C(O)), 77.9 (C), 71.4 (CH), 70.9 (CH), 43.8 (CH$_2$), 41.6 (CH$_2$); elemental analysis calcd (%) for C$_{16}$H$_{18}$N$_2$O$_2$Cl$_2$Fe: N 7.06, C 48.39, H 4.57; found: N 6.91, C 48.17, H 4.61.

2.3.6 Synthesis of 8 (fc(C{O}NHCH$_2$CH$_2$SH)$_2$)

0.45 g (1.1 mmol) of **7** was dissolved in 30 mL of THF and cooled to -10 ˚C. S(SiMe$_3$)$_2$ (0.72 mL, 3.4 mmol) was added, followed by TBAF (0.66 g, 2.5 mmol) in 10 mL THF. The reaction mixture was stirred at -10 ˚C for 10 mins, the cooling bath was removed and the reaction mixture was stirred for ~ 24 hours at RT. The THF was removed under vacuum and 30 mL of CH$_2$Cl$_2$ was used to dissolve the residue. Degassed, deionized water (5 × 30 mL) was used to wash the solution, which was subsequently dried over MgSO$_4$. Filtration followed by solvent removal under vacuum yielded **7** as a dark orange solid. Yield = 0.15 g (34%) ^{1}H NMR (400 MHz, CDCl$_3$, 23 ˚C): δ = 7.09 (s, 2H, NH), 4.54 (m, 4H, CH), 4.40 (m, 4H, CH), 3.59 (dt, ^3J = 4.0 Hz, ^2J = 4.0 Hz, 4H, CH$_2$), 2.83 (dt, ^3J = 4.8 Hz, ^2J = 5.2Hz, 4H, CH$_2$), 1.53 (t, ^3J = 5.2 Hz, 2H, SH). ^{13}C{^{1}H} NMR (100.5 MHz, CDCl$_3$): δ = 170.7 (C(O)), 78.4 (C), 71.1 (CH), 70.9 (CH), 42.8 (CH$_2$), 24.6 (CH$_2$); HRMS: *m/z*: calcd for C$_{16}$H$_{20}$Fe$_1$N$_2$O$_2$S$_2$: 392.03157; found: 392.03238.

2.4 Results and Discussion

2.4.1 Synthesis

In order to prepare the bidentate ferrocenyl chalcogen reagents with an ester or amide functionality, previous work of making the mono substituted analogs was consulted.[11] The synthesis of both the di-ester and the di-amide were started from 1,1'-ferrocene dicarboxylic acid, which was prepared according to literature methods.[13]

For the ester **1**, 1,1'-ferrocene dicarboxylic acid was first converted into 1,1'-ferrocene dicarbonyl chloride[15] and then coupled with 2-bromoalcohol to yield compound **1** (fc(C{O}OCH₂CH₂Br)₂). 1,1'-Ferrocene dicarbonyl chloride was unstable even in the solid state and is best used immediately after preparation. Compounds **2** (fc(C{O}OCH₂CH₂Br)COOH) and **3** ((fc(C{O}O{O}C))₂) were also isolated from the reaction and are formed due to the partial hydrolysis of 1,1'-ferrocene dicarbonyl chloride in the ester coupling process (Scheme 2.1). While compound **1** is the expected product, compound **2** was also very attractive and opens a window for potential different functional group addition on ferrocene moiety.
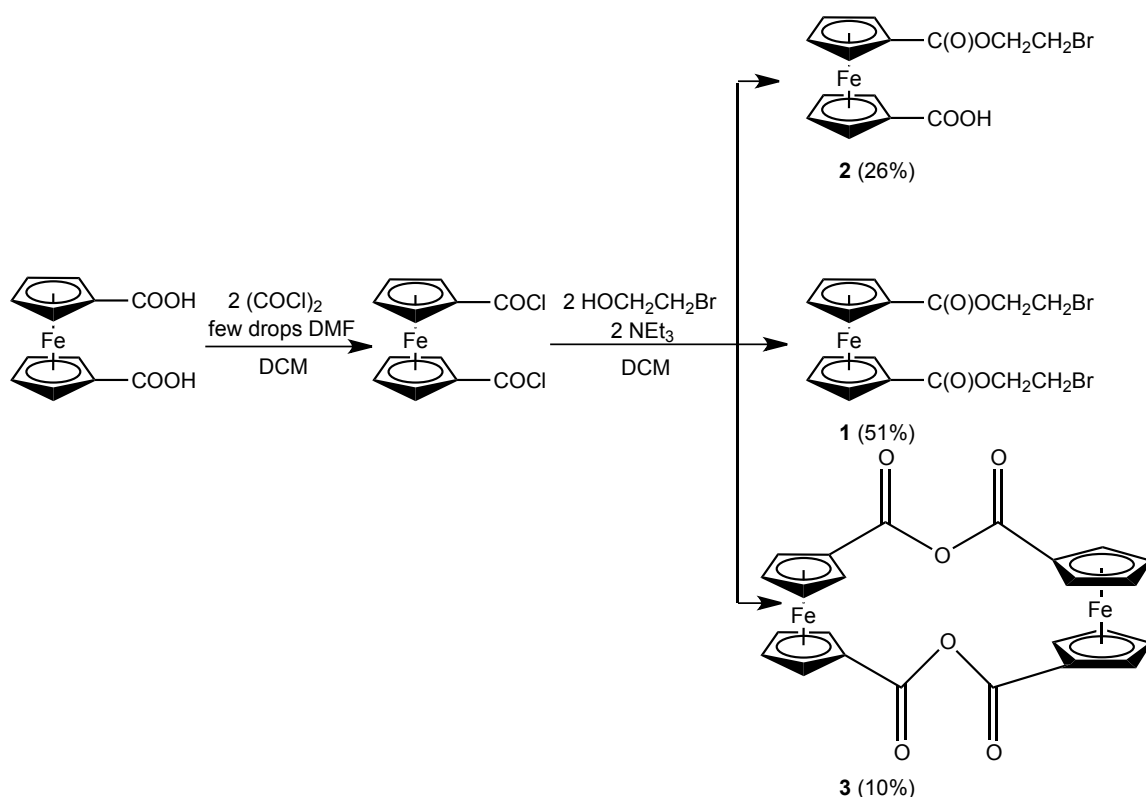
Scheme 2.1 Synthesis of fc(C{O}OCH₂CH₂Br)₂ (**1**), fc(C{O}OCH₂CH₂Br)COOH (**2**) and (fc(C{O}O{O}C))₂ (**3**)

Compound **4** could be prepared from **1** through the addition of tetrabutylammonium fluoride hydrate (TBAF) with S(SiMe$_3$)$_2$ in THF at -10 $^\circ$C. TBAF must never be in excess relative to S(SiMe$_3$)$_2$, otherwise S^{2-} formation can lead to the formation of additional products. A slight excess of S(SiMe$_3$)$_2$/TBAF (2.2 equiv.) ensures a higher purity and yield of compound **4**. Tetrabutylammonium bromide was subsequently removed from the reaction mixture through precipitation with heptane and filtration. Compound **4** could be isolated at this step as a red, oily solid through removal of the solvent *in vacuo*. (Scheme 2.2)
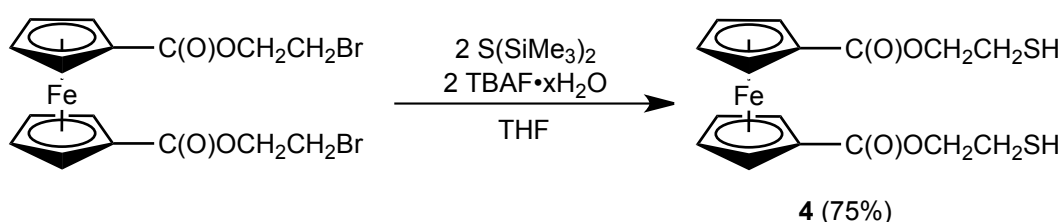
Scheme 2.2 Synthesis of fc(C{O}OCH$_2$CH$_2$SH)$_2$ (**4**)

Following established methods for the preparation of [AgSR],[16] attempts were made to prepare **5** ([fc(C{O}OCH$_2$CH$_2$SAg)$_2$]$_n$) by adding a solution of silver nitrate (AgNO$_3$) in CH$_3$CN to a solution of **4** in CH$_3$CN, together with NEt$_3$. However, the color of the solution changed to dark grey in a short period of time, which suggested oxidation of **4**. A reasonable explanation was the nitrate group serving as an oxidizer even in a neutral solution. An alternate silver source was used in the form of silver trifluoromethanesulfonate. This yielded a yellow precipitate that formed immediately. While **4** was air stable, **5** had modest sensitivity to air and could be stored under nitrogen for further use. (Scheme 2.3)
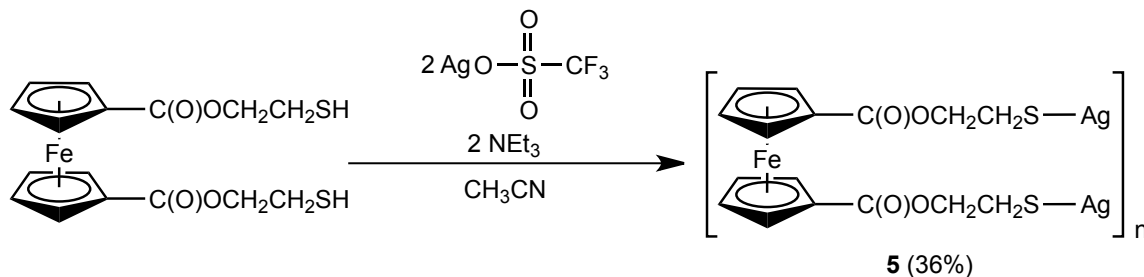
Scheme 2.3 Synthesis of $[fc(C\{O\}OCH_2CH_2SAg)_2]_n$ (**5**)

Compound **6** was synthesized by using the similar method for making $Fc(C\{O\}OCH_2CH_2SSiMe_3)$, from the dithiol with NEt_3 and $ClSiMe_3$. (Scheme 2.4)
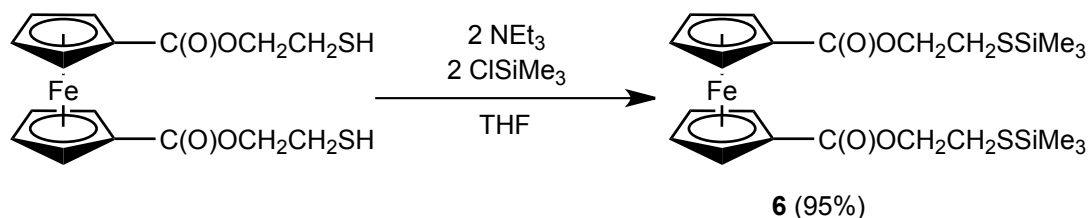
Scheme 2.4 Synthesis of $fc(C\{O\}OCH_2CH_2SSiMe_3)_2$ (**6**)

Attempts to synthesize the disubstituted $1,1'$-$fc(C(O)NHCH_2CH_2Cl)_2$ (**7**) via modification of the method used for monosubstituted $FcC(O)NHCH_2CH_2Cl$,[11] (i.e. the addition of 2.5 equivalents of 2-chloroethylisocyanate to ferrocene with 2.5 equivalents of aluminum chloride) ultimately resulted in the formation of only N-(2-chloroethyl)ferrocenylcarboxamide, with no further substitution reaction taking place. Thus **7** was synthesized starting from $1,1'$- ferrocene dicarboxylic acid and 2-chloroethanol. *N,N'*-Dicyclohexylcarbodiimide (DCC) and 1-hydroxybenzotriazole (HoBt) were used as amide coupling reagents and **7** was successfully prepared using this method. However, the removal of traces of DCC-urea from **7** proved to be difficult. The

synthesis was repeated using N-(3-dimethylaminopropyl)-N'-ethylcarbodiimide (EDC) as
an amide coupling reagent, yielding pure **7** after column chromatography.

$$2\ H_2NCH_2CH_2Cl \cdot HCl$$
$$2\ EDC \cdot HCl$$
$$HoBt$$
$$6\ NEt_3$$
$$DCM$$

Fe — COOH, COOH → Fe — C(O)NHCH$_2$CH$_2$Cl, C(O)NHCH$_2$CH$_2$Cl

7 (43%)
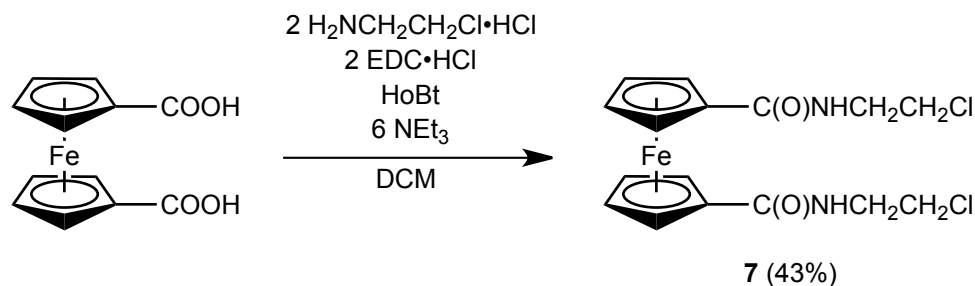
Scheme 2.5 Synthesis of fc(C{O}NHCH$_2$CH$_2$Cl)$_2$ (**7**)

Compound **8** was prepared following a method of synthesizing **4**. S(SiMe$_3$)$_2$ and TBAF
were added to a solution of **7** to yield **8**. **8** (ferrocenyl amide dithiol) was very sensitive to
air.

$$2\ S(SiMe_3)_2$$
$$2\ TBAF \cdot xH_2O$$
$$THF$$

Fe — C(O)NHCH$_2$CH$_2$Cl, C(O)NHCH$_2$CH$_2$Cl → Fe — C(O)NHCH$_2$CH$_2$SH, C(O)NHCH$_2$CH$_2$SH

8 (34%)
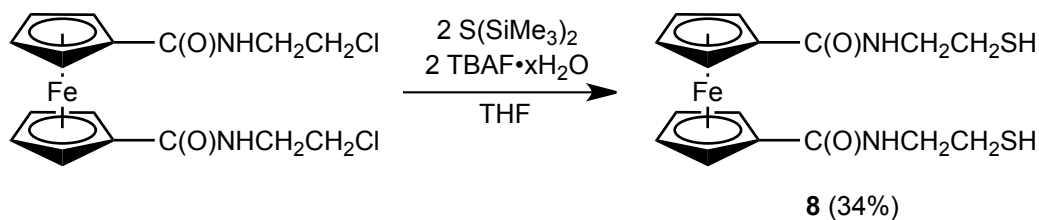
Scheme 2.6 Synthesis of fc(C{O}NHCH$_2$CH$_2$SH)$_2$ (**8**)

2.4.2 X-ray crystallography

High quality crystals of **1** were obtained through slow evaporation of a solution of **1** in
diethyl ether and hexanes. Compound **1** (Figure 2.1) crystallizes in the monoclinic space
group $P2_1$ with two molecules in the unit cell. The cyclopentadienyl (Cp) rings defined
by C(1)-C5 and C6-C10 are almost perfectly parallel. O1 and O2 are distended out of the

plane of the Cp ring by 0.017 and 0.188 Å, and O3 and O4 are rotated out of the plane defined by their respective Cp rings by 0.089 and 0.121 Å. The iron-carbon (2.025(4)-2.062(4) Å) and carbon-carbon (1.415(5)-1.438(5) Å) bond lengths in the Cp rings are in accord with those observed in free ferrocene.[17] The two substituted chains of **1** are staggered, where the angle formed by C14 and C6 with C(1) and C11 is 139.62°.

There are five intermolecular hydrogen bonds in the packing of compound **1**, two formed from O1 (O1-H16B and O1-H12A), two formed from O3 (O3-H13A and O3-H15B) and another one formed from Br2 (Br2-H4), which have stabilized the crystal and surely influenced the packing. Some selected bond lengths and angles for compound **1** are listed in Table 2.1.

Table 2.1 Selected bond lengths [Å] and angles [°] for **1**

C11-O1	1.218(5)	O1-C11-O2	123.2(4)
C11-O2	1.350(5)	C11-O2-C12	115.9(3)
O2-C12	1.439(5)	C12-C13-Br1	112.0(3)
C13-Br1	1.954(4)	O3-C14-O4	123.3(3)
C14-O3	1.207(5)	C14-O4-C15	115.4(3)
C14-O4	1.360(4)	C15-C16-Br2	112.1(3)
O4-C15	1.457(5)		
C16-Br2	1.955(4)		

X-ray-quality crystals of **2** were obtained through slow evaporation of a solution of **2** in diethyl ether and hexanes. Compound **2** (Figure 2.2) crystallizes in the monoclinic space group $P2_1/n$ with four molecules in the unit cell. The two substituted chains of **2** are also staggered, like **1,** where the angle formed by C11 and C(1) with C14 and C6 is 136.41°.
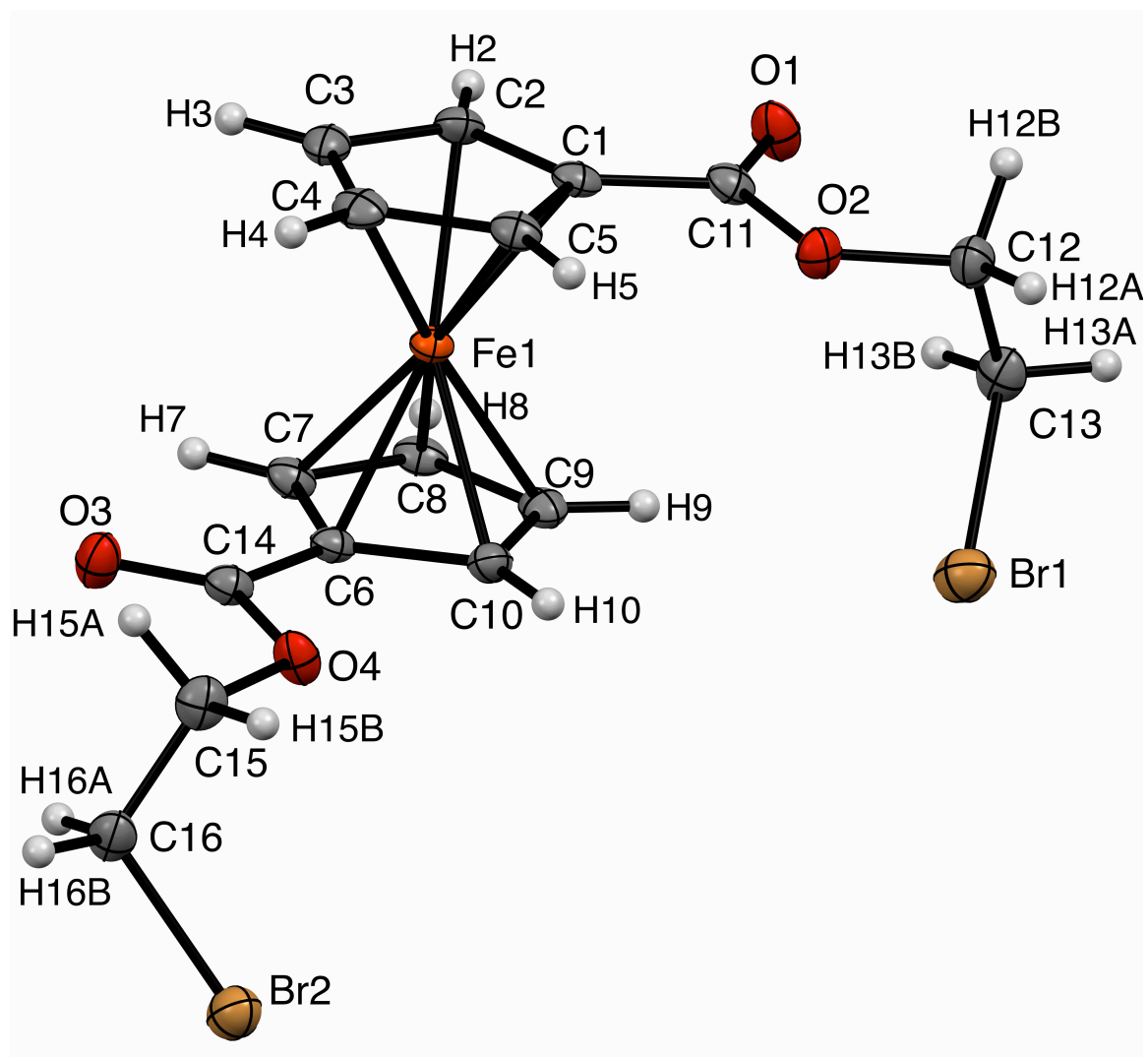
Figure 2.1 Molecular structure of **1**. Thermal ellipsoids are drawn at 50%.
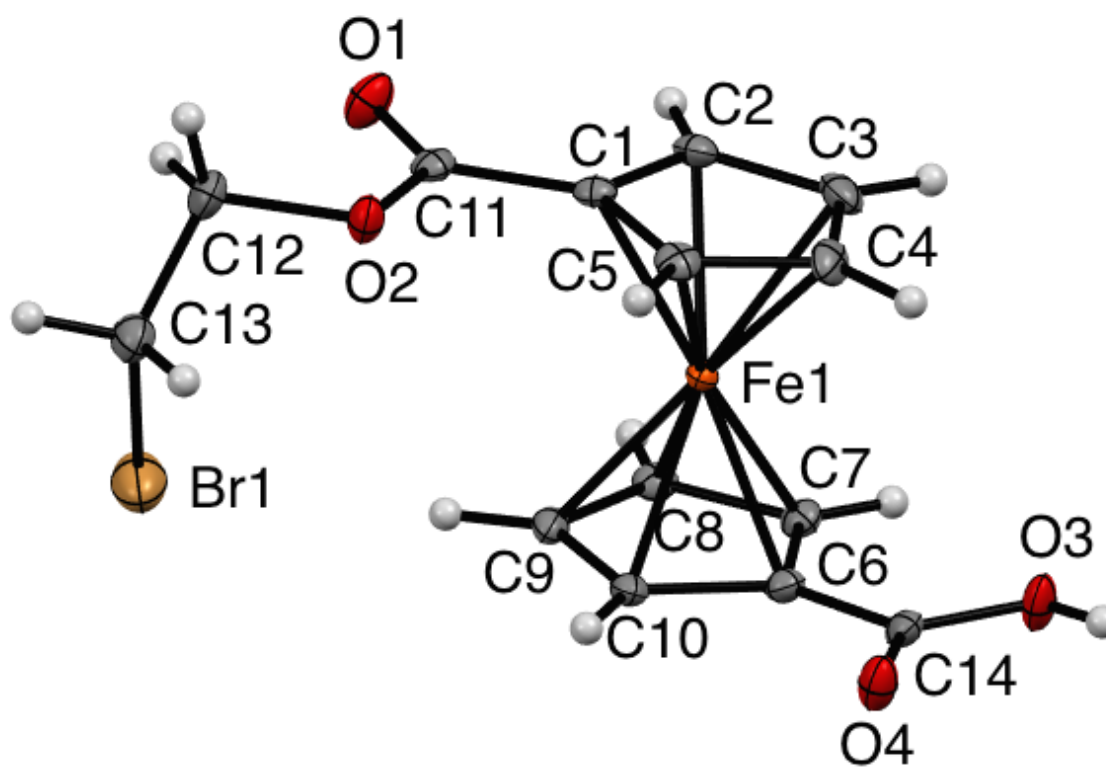
Figure 2.2 Molecular structure of **2**. Thermal ellipsoids are drawn at 50%.

Table 2.2 Selected bond lengths [Å] and angles [°] for **2**

C11-O1	1.207(3)	O1-C11-O2	124.4(3)
C11-O2	1.350(3)	C11-O2-C12	117.4(2)
O2-C12	1.444(3)	C12-C13-Br1	111.5(2)
C13-Br1	1.949(3)	O4-C14-O3	124.2(3)
C14-O4	1.226(4)		
C14-O3	1.317(3)		

As shown in Figure 2.3, compound **2** displays two strong H-bonding interactions. Each molecule interacts with one other neighboring molecule to form a "dimer" via the interaction of two carboxylic acid groups.
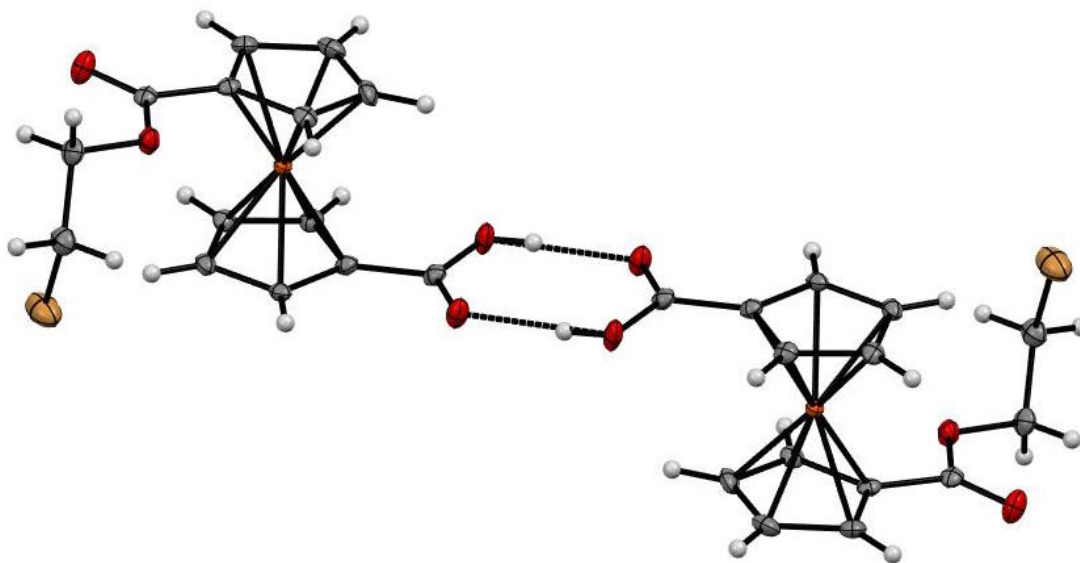
Figure 2.3 Hydrogen bonding interactions between molecules of **2**.

X-ray-quality crystals of **3** were obtained through slow evaporation of a solution of **3** in diethyl ether and ethyl acetate. Compound **3** (Figure 2.4) crystallizes in the monoclinic space group $P2_1/n$ with two molecules in the unit cell. There are two ferrocene units in

compound **3**, the two ferrocene units are not horizontal, but almost parallel, with the plane formed by C1A, C2A, C3A, C4A and C5A in one ferrocene moiety is out of the plane formed by C6, C7, C8, C9 and C10 in another ferrocene moiety by 0.540 Å. The two substituted chains in both ferrocene units of **3** are staggered, whereas the angles formed by C7 and C12A with C1 and C11, C1A and C11A with C7A and C12 are both 74.37°.
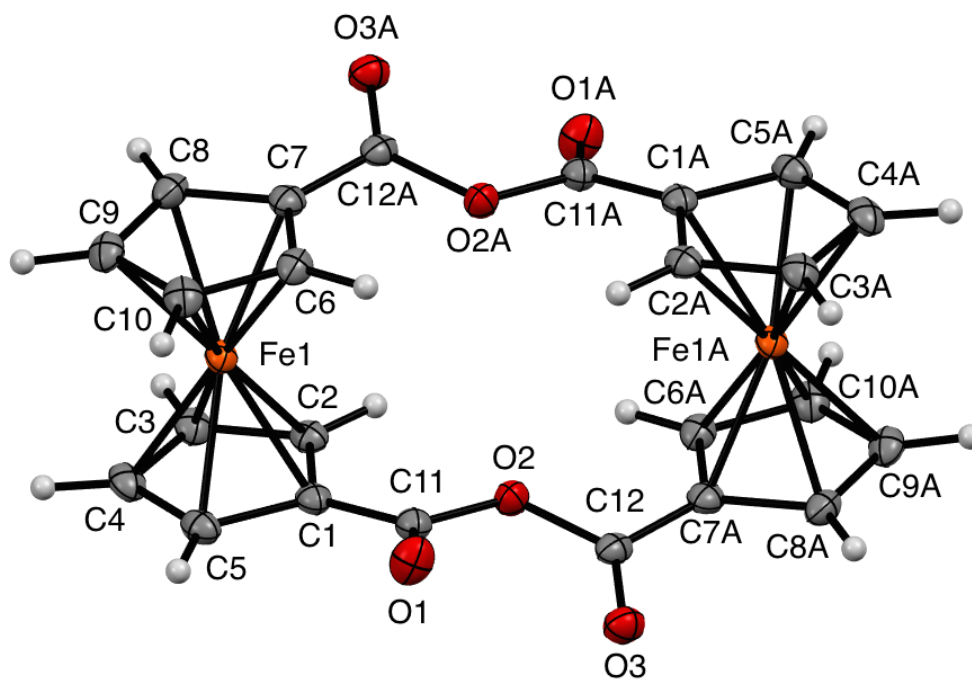
Figure 2.4 Molecular structure of **3**. Thermal ellipsoids are drawn at 50%.

Table 2.3 Selected bond lengths [Å] and angles [°] for **3**

C7-C12	1.471(4)	O1-C11-C(1)	125.7(2)
C12-O3	1.193(3)	O1-C11-O2	124.2(2)
C12-O2	1.391(3)	O2-C11-C1	110.1(2)
O2-C11	1.390(3)	C11-O2-C12	120.9(2)
C11-O1	1.200(3)	O3-C12-O2	124.3(2)
C11-C(1)	1.472(4)	O3-C12-C7	125.4(2)
		O2-C12-C7	110.2(2)

2.4.3 NMR Spectroscopy

The synthesis of bidentate ferrocenyl dithiol reagents was easily followed using NMR spectroscopy. The ^{1}H NMR spectrum of fc(C{O}OCH$_2$CH$_2$Br)$_2$ **1** (Figure. 2.5) shows four well resolved signals at 4.89, 4.54, 4.48 and 3.65 ppm, with the signals at 4.54 and 3.65 ppm related to the methylene protons of the –CH$_2$CH$_2$- spacer. Synthesized from **1**, compound fc(C{O}OCH$_2$CH$_2$SH)$_2$ **4** shows five signals at 4.85, 4.45, 4.36, 2.87 and 1.60 ppm (Figure 2.6). The signal at 1.60 ppm is assigned to the –SH proton. With the two signals from cyclopentadienyl rings at 4.85 and 4.45 ppm almost unchanged, the signals from the methylene protons of the –CH$_2$CH$_2$– spacer are both shifted upfield in **4** as –SH is a weaker electron withdrawing group compared with –Br.

The ^{1}H NMR spectrum of fc(C{O}NHCH$_2$CH$_2$Cl)$_2$ **7** shows four signals at 7.04, 4,57, 4.42 and 3.76 ppm (Figure 2.7), with the signal at 7.04 ppm assigned to the amide proton and 3.76 ppm related to the methylene protons of the –CH$_2$CH$_2$– spacer. While the signals of the methylene protons are separated in **1**, they are merged in **7** due to the influence of the amide group. Using **7** as precursor in the synthetic procedure, fc(C{O}NHCH$_2$CH$_2$SH)$_2$ **8** shows six signals at 7.09, 4.54, 4.40, 3.59, 2.83 and 1.53 ppm, respectively (Figure 2.8). The signal at 1.53 ppm is assigned to the –SH proton, which is consistent with that in **1**. The substitution of –Cl with –SH lead the signal of the methylene protons in the –CH$_2$CH$_2$– spacer that is closer to –SH shifted upfield, as –SH
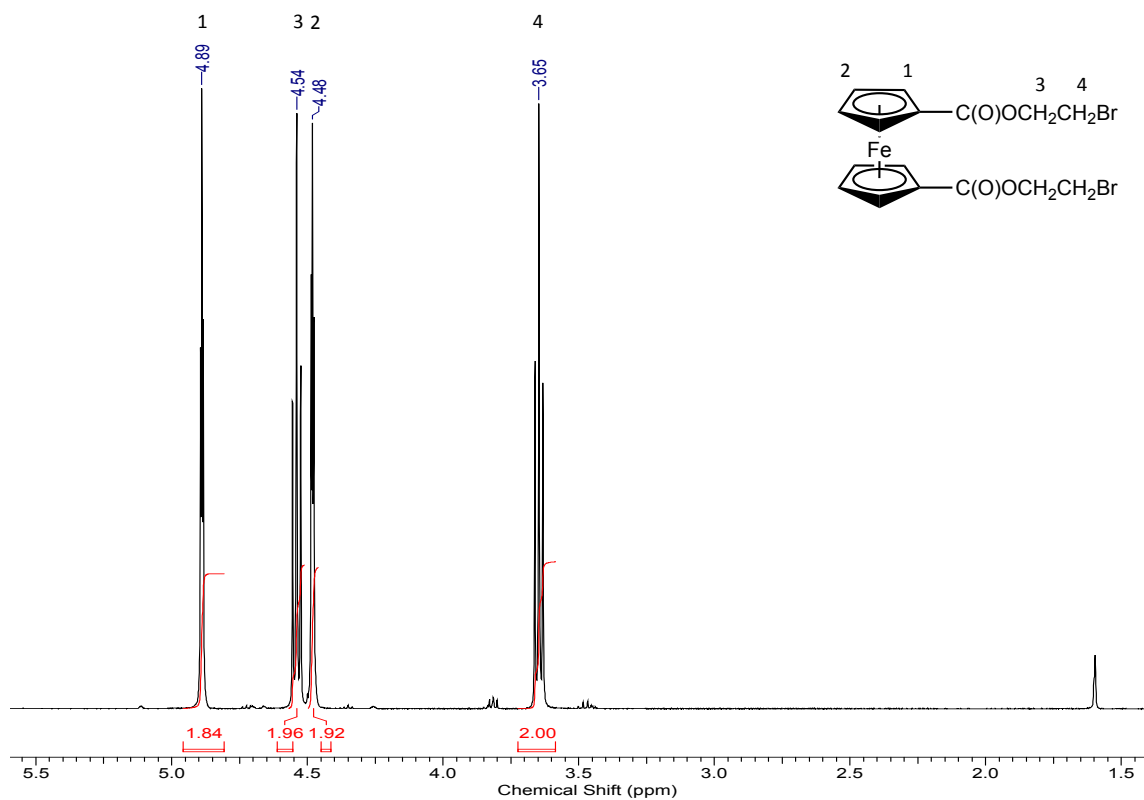
Figure 2.5 ^{1}H NMR spectrum of fc(C{O}OCH$_2$CH$_2$Br)$_2$ **1**
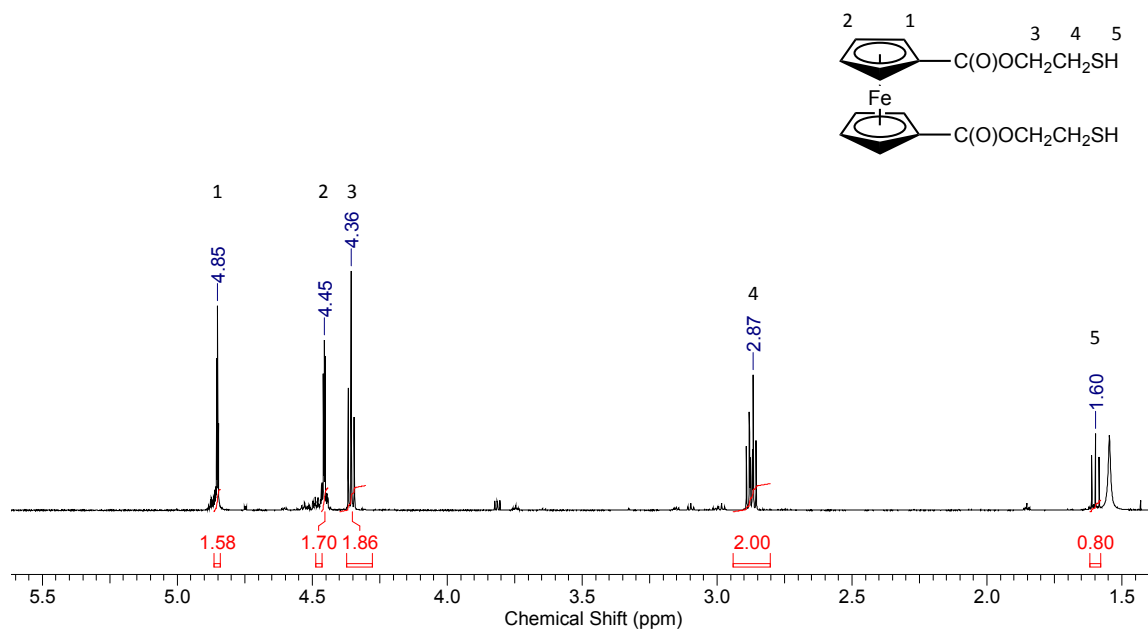
Figure 2.6 ^{1}H NMR spectrum of fc(C{O}OCH$_2$CH$_2$SH)$_2$ **4**

is a weaker electron withdrawing group. Signals of the other methylene protons are almost unchanged. In this case, the merged signals of two methylene protons in **7** are separated well in **8**, which is a signature related to **8**.
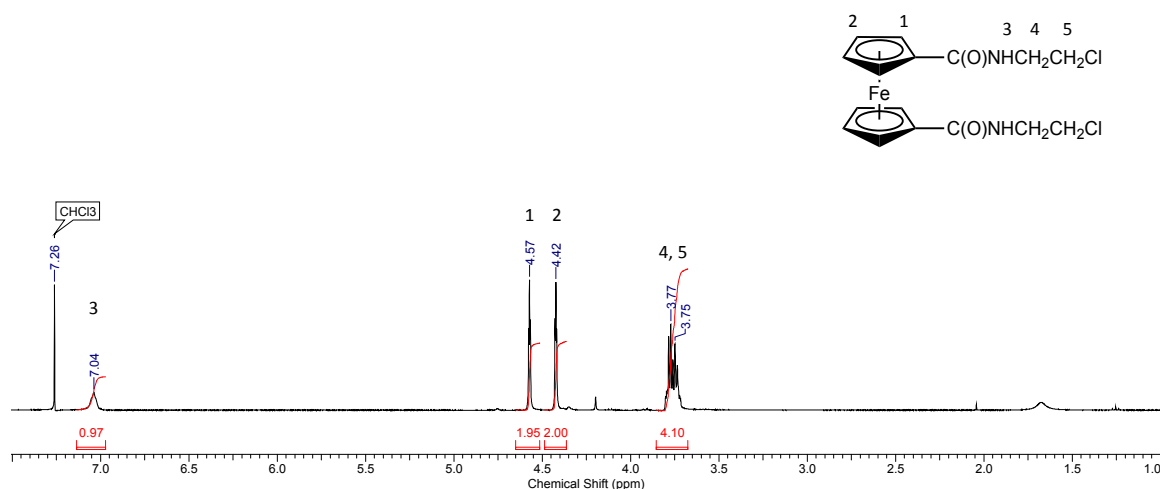
Figure 2.7 ^{1}H NMR spectrum of fc(C{O}NHCH$_2$CH$_2$Cl)$_2$ **7**
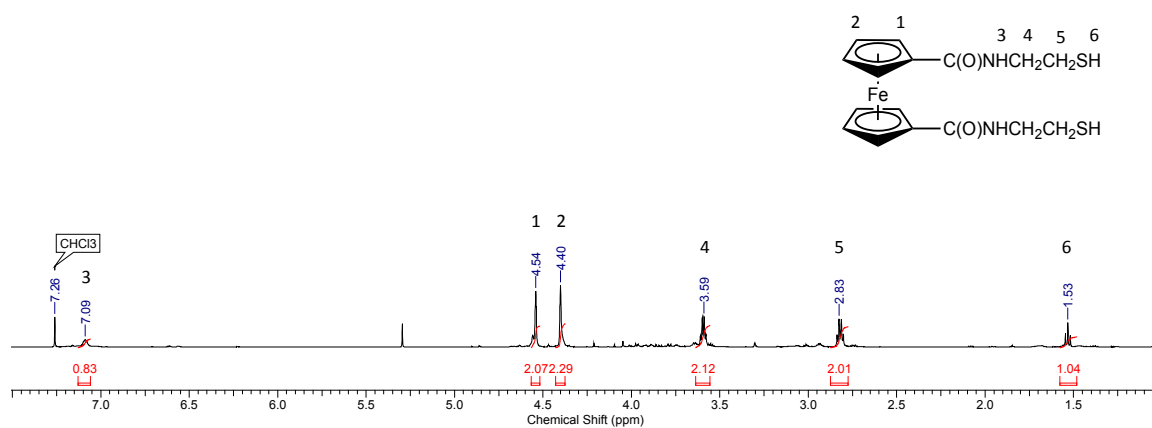
Figure 2.8 ^{1}H NMR spectrum of fc(C{O}NHCH$_2$CH$_2$SH)$_2$ **8**

2.4.4 UV-Vis Absorption Spectroscopy

The solution electronic absorption spectra of compounds **1**, **2**, **4**, and **6** are presented in Figure 2.9 while that of **7** and **8** are presented in Figure 2.10. For **1**, the spectrum shows three characteristic maxima: a broad maximum at 307 nm, a shoulder at 345 nm, and a broad absorption centered at 450 nm. The three absorption peaks are typical of similar substituted ferrocenes that contain a ferrocene-carbonyl portion, such as acetylferrocene, with the absorption at 345 nm arising due to the presence of the ferrocene-carbonyl moeity.[18, 19, 20] A small red shift is observed for the lowest-energy transition (451 nm) compared with that of the free ferrocene.[18, 19] Due to the structurally similarity, the absorption maxima of compound **2**, **4** and **6** showed no significant differences compared with that of **1**, while compound **6** showed smaller ε at the related area compared with the other three. Molar absorption coefficients data of compound **1**, **2**, **4**, and **6** are shown in Table 2.4.
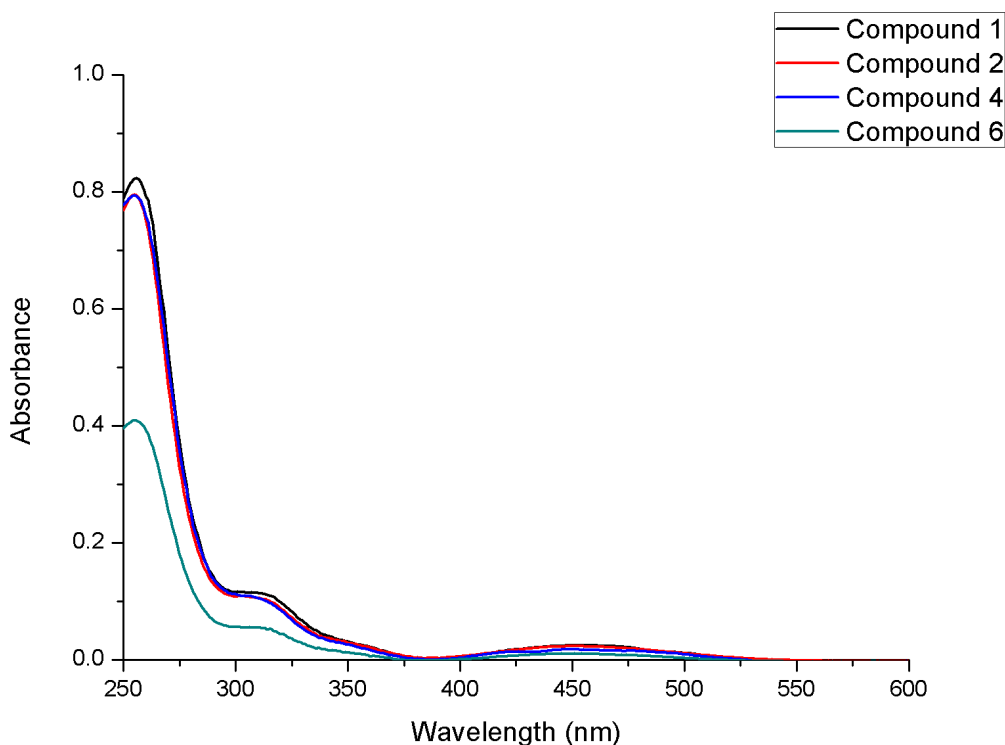
Figure 2.9 Absorption spectra of **1**, **2**, **4** and **6** (8.0 x 10^{-5} M)

Table 2.4 Molar absorption coefficients, ε, at the corresponding wavelengths, λ, of compound **1**, **2**, **4** and **6**.

	λ[nm] (ε/[Lmol^{-1}cm^{-1}])			
1[a]	256 (1.0 x 10^4)	307 (1.4 x 10^3)	345 (4.5 x 10^2)	451 (3.1 x 10^2)
2[a]	255 (9.9 x 10^3)	308 (1.3 x 10^3)	346 (4.2 x 10^2)	452 (2.9 x 10^2)
4[a]	255 (9.9 x 10^3)	307 (1.3 x 10^3)	346 (3.8 x 10^2)	446 (2.2 x 10^2)
6[a]	256 (5.1 x 10^3)	306 (7.0 x 10^2)	343 (2.1 x 10^2)	451 (1.3 x 10^2)

[a] 8.0 x 10^{-5} M.

For compound **7**, the spectrum shows three characteristic maxima: a shoulder at 306 nm, a broad absorption at 345 nm and a second broad absorption at 440-450 nm. The maxima at 449 nm can be assigned to the symmetry forbidden d-d transition in the ferrocenyl moiety, according to the report of other ferrocenyl amides.[21] The absorption spectrum of compound **8** was similar to that of compound **7** due to the similarity of the molecular structure, but with smaller ε. Molar absorption coefficients data of compound **7** and **8** are shown in Table 2.5.

Table 2.5 Molar absorption coefficients, ε, at the corresponding wavelengths, λ, of compound **7** and **8**.

	λ[nm] (ε/[Lmol^{-1}cm^{-1}])			
7[a]	253 (7.7 x 10^3)	306 (8.3 x 10^2)	345 (2.8 x 10^2)	449 (1.8 x 10^2)
8[a]	256 (3.3 x 10^3)	306 (4.2 x 10^2)	345 (1.4 x 10^2)	450 (51)

[a] 8.0 x 10^{-5} M.

Figure 2.10 Absorption spectra of **7** and **8** (8.0 x 10^{-5} M)

2.5 Conclusion

The bidentate ferrocenyl dithiol reagents with both the ester and amide functionalities have been successfully prepared. Compound **1** was prepared while **2** and **3** isolated as byproducts due to partial hydrolysis during reaction process. **1** was used in subsequent reaction for preparing **5** and efforts have been given to improve **5**'s purity. Bidentate ferrocenyl ester dithiol **5** was proven air stable and can be transferred into a silver thiolate coordination polymer for cluster formation. Compound **7** was successfully made pure using a different synthetic route from its monodentate analog and transferred into the bidentate ferrocenyl amino dithiol. The UV-Vis absorption spectrum for compound **1**, **2**, **4** and **5** exhibited absorption maxima that are typical for ferrocenyl carboxylate compounds while **7** and **8** shown UV curves common for ferrocenyl amino compounds.

2.6 References for Chapter 2

1. Siemeling, U.; Rother, D.; Bruhn, C.; Fink, H.; Weidner, T.; Träger, F.; Rothenberger, A.; Fenske, D.; Priebe, A.; Maurer, J.; Winter, R. *J. Am. Chem. Soc.* **2005**, *127*, 1102.

2. Mochida, T.; Shimizu, F.; Shimizu, H.; Okazawa, K.; Sato, F.; Kuwahara, D. *J. Organomet. Chem.* **2007**, *692*, 1834.

3. Newkome, G. R.; He, E.; Moorefield, C. N. *Chem. Rev.* **1999**, *99*, 1689.

4. Roussier, R.; Abdulla, A.; Gautheron, B. *J. Organomet. Chem.* **1987**, *332*, 165.

5. Breti, B.; Breuninger, D. *Synthesis* **2005**, *16*, 2782.

6. Wallbank, A. I.; Borecki, A.; Taylor, N. J.; Corrigan, J. F. *Organometallics* **2005**, *24*, 788.

7. Nitschke, C.; Fenske, D.; Corrigan, J. F. *Inorg. Chem.* **2006**, *45*, 9394.

8. Wallbank, A. I.; Corrigan, J. F. *Chem. Commun.* **2001**, 377.

9. Brown, M. J.; Corrigan, J. F. *J. Organomet. Chem.* **2004**, *689*, 2872.

10. Ahmar, S.; MacDonald, D. G.; Vijayaratnam, N.; Battista, T. L.; Workentin, M. S.; Corrigan, J. F. *Angew. Chem. Int. Ed.* **2010**, *49*, 4422.

11. MacDonald, D. G.; Eichhöfer, A.; Campana, C. F.; Corrigan, J. F. *Chem. Eur. J.* **2011**, *17*, 5890.

12. Taher, D.; Wallbank, A. I.; Turner, E. A.; Cuthbert, H. L.; Corrigan, J. F. *Eur. J. Inorg. Chem.* **2006**, 4616.

13. Laufer, R.; Veith, U.; Taylor, N. J.; Snieckus, V. *Can. J. Chem.* **2006,** *84,* 356.

14. Sheldrick, G. M. Acta Cryst. 2008, A64, 112.

15. Rogers, R. S. *Tetrahedron Lett.* **1992**, *33*, 7473.

16. Teo, B. K.; Xu, Y.; Zhong, B.; He, Y.; Chen, H.; Qian, W.; Deng, Y.; Zou, Y. *Inorg. Chem.* **2001,** *40,* 6794.

17. Dunitz, J.; Orgel, L.; Rich, A.; *Acta Crystallogr.* **1956**, *9*, 373.

18. Fery-Forgues, S.; Delavaux-Nicot, B. *J. Photochem. Photobiol. A* **2000**, *132*, 137.

19. Barr, T. H.; Watts, W. E. *J. Organomet. Chem.* **1968**, *15*, 177.

20. Nielson, D.; Farmer, M.; Eyring, H. *J. Phys. Chem.* **1976**, *80*, 717.

21. Heinze, K.; Schlenker, M. *Eur. J. Inorg. Chem.* **2004**, 2974.

Chapter 3
Preparation and Characterization of A New Di(thiaethyl)ferrocenyldicarboxylate Metal Cluster

3.1 Introduction

The preparation of molecular architecture containing multiple ferrocenyl units has been attracting attention from researchers. The three most commonly used supporting frameworks are polymers,[1] dendrimeric frameworks[2] and inorganic cores.[3, 4] Among the three, dendrimeric frameworks are the most favored due to their large surface-area-to-volume ratio, but the drawback is they are usually difficult to prepare. Inorganic cores are another class of material which can be used for the support, and gold nanoparticles and metal-chalcogenide clusters are the most common in this category. Gold nanoparticles are easy to prepare; however, examples reported so far are gold nanoparticles with multiple ferrocene units but for which structural characterization is lacking. Using metal-chalcogenide clusters as a support for ferrocenyl ligands can yield monodisperse species whose structures can be determined by single X-ray diffraction.[5, 6] These materials have the advantage of zero size distribution. Several examples have been reported with the incorporation of multiple ferrocenyl units with metal-chalcogen core; however, these molecules are all relatively small and examples with high-nuclearity cores are still rare.[5, 6]

The use of silyated reagents has proven to be fruitful in the preparation of metal chalcogenide clusters;[7] many examples have been reported by applying this strategy. Recently, Fenske and co-workers reported a complementary synthetic route for metal chalcogenide clusters by using silver thiolate coordination polymers (AgSR) as precursors.[8, 9] Several examples have been reported, including the largest structurally characterized silver sulfide cluster reported to date, $[Ag_{490}S_{188}(StC_5H_{11})_{114}]$.[9] This is a new powerful route in metal-chalcogen chemistry, especially for the synthesis of large discrete molecules with high-nuclearity cores. Due to the tunability of "R", in principle it is possible to introduce different functionalities onto the surface of the silver sulfide, however this strategy has yet to be probed in depth.

Previously, the silylated reagents $CpFe(\eta^5\text{-}C_5H_4COXCH_2CH_2ESiMe_3)$ (X = O, NH; E = S, Se)[6] have been prepared and their use in cluster formation has been developed. The cluster $[Ag_{14}(PPh_3)_6S(SCH_2CH_2O\{O\}CFc)_{12}]$ was successfully prepared and structurally characterized. Although attempts to produce higher-nuclearity clusters with a ferrocene rich surface resulted in the formation of crystalline materials,[10] such as $[Ag_{36}S_9(SCH_2CH_2O\{O\}CFc)_{18}(PPh_3)_3]$, $[Ag_{100}Se_{17}(SeCH_2CH_2O\{O\}CFc)_{66}(PPh_3)_{10}]$ and $[Ag_{180}Se_{54}(SeCH_2CH_2O\{O\}CFc)_{72}(PPh_3)_{14}$, whose compositions could be formulated on the basis on elemental analysis, high resolution transmission electron microscopy and dynamic light scattering. The hypothesis was made that the limitation of only one ligating point of monodentate ferrocenyl-chalcogen reagents led to the problem of generating single crystals of these materials. Therefore, the analogous bidentate ferrocenyl-dithiol ligands were prepared and targeted for cluster formation. The successful synthesis of the bidentate ferrocenyl-dithiol ligand $1,1'\text{-}fc(C\{O\}OCH_2CH_2SH)_2$ (**4**) and the corresponding coordination polymer $fc(C\{O\}OCH_2CH_2SAg)_2$ (**5**) have been presented in Chapter 2, and the reactivity of the coordination polymer for the preparation of high-nuclearity cluster $[Ag_{74}S_{19}(dppp)_6(fc(C\{O\}OCH_2CH_2S)_2)_{18}]$ (dppp = 1, 3-bis(diphenylphosphino)propane) (**9**) will be discussed in this chapter.

3.2 Materials and Methods

3.2.1 Starting Materials

All synthetic and handling procedures were performed using standard double manifold Schlenk line techniques under a dry and high purity nitrogen atmosphere, or in a MBraun inert atmosphere (N_2) glovebox. Dichloromethane (CH_2Cl_2) was dried and distilled over P_2O_5. 1,3-Bis(diphenylphosphino)propane (dppp) and silver acetate (AgOAc) were purchased from Alfa Aesar. Tetrabutylammonium hexafluorophosphate (NBu_4PF_6) and tetrabutylammonium bisulfate (NBu_4HSO_4) were purchased from Aldrich. The silyated reagent $S(SiMe_3)_2$ was prepared according to literature procedures.[11] Reagent $[fc(C\{O\}OCH_2CH_2SAg)_2]_n$ (**5**) was prepared as described in Chapter 2.

3.2.2 Characterization

Single crystal data were collected using a Canadian Macromolecular Crystallography Facility beamline (CMCF-BM or 08B1-1) at the Canadian Light Source (CLS). 08B1-1 is a bending magnet beamline with a Si (111) double crystal monochromator. 2-dimensional (2D) data was obtained using a Rayonix MX300HE detector with an active area of 300 mm x 300 mm. The patterns were collected at an energy of 18 keV (λ = 0.68877Å), a capillary-detector distance of 150 mm and a temperature of 110 (1) K. The structure was solved with direct methods and refined using the SHELX suite of crystallographic software[12] by Dr. John F. Corrigan.

Elemental analysis was performed by Laboratoire d'analyse élémentaire, Université de Montréal (Montréal, Canada). UV/Vis absorption spectra were recorded on a Varian Cary 300 Bio UV/Vis spectrophotometer. Fluorescence experiments were performed using a PTI QuantMaster. A BAS 100 electrochemical workstation using a 3-electrode system, with platinum working electrode or glassy carbon working electrode (mentioned specifically in different experiments), platinum flag counter electrode, and a Ag/AgCl reference electrode (Fisher Accumet Cat # 13-620-53, in 4M KCl) with 0.1 M NBu_4PF_6 in CH_2Cl_2 as the supporting electrolyte were used for electrochemical measurements.

3.3 Experimental

3.3.1 Synthesis and characterization of $[Ag_{74}S_{19}(dppp)_6(fc(C\{O\}OCH_2CH_2S)_2)_{18}]$ (9)

The silver thiolate coordination polymer (**5**) (0.10 g, 0.16 mmol) was dissolved in 20 mL CH_2Cl_2 with dppp (0.14 g, 0.33 mmol) by stirring for 1.5 hours to yield an orange solution. $S(SiMe_3)_2$ (0.01 mL, 0.05 mmol) was then added and stirred for two hours at room temperature. The resultant solution was dark red in color. The reaction mixture was layered with 20 mL Et_2O and stored in the dark for 3-4 days to yield dark red, block like single crystals of **9**. The structure was identified by X-ray crystallography to be $[Ag_{74}S_{19}(dppp)_6(fc(C\{O\}OCH_2CH_2S)_2)_{18}]$. Yield: 30 mg (63%).

Elemental analysis calcd (%) for $Ag_{74}S_{55}Fe_{18}C_{450}H_{444}P_{12}O_{72}$: C 29.83, H 2.47, S 9.70; found: C 28.97, H 2.32, S 9.63. Due to the poor solubility of **9** in common organic solvents, no NMR spectra could be obtained.

3.4 Results and Discussion

3.4.1 Synthesis of $[Ag_{74}S_{19}(dppp)_6(fc(C\{O\}OCH_2CH_2S)_2)_{18}]$ (9)

The synthetic strategy using silver thiolate coordination polymers[8, 9] as precursors for the preparation of metal chalcogen clusters had inspired new potential routes for incorporation ferrocenyl units onto the surface of clusters. The synthesis of the monodentate ferrocenyl-chalcogen ligands $Fc(C\{O\}XCH_2CH_2ESSiMe_3)$ (X = O, NH; E = S, Se) and their abilities in cluster formation[6, 10] prompted us to investigate the capacity of a bidentate ferrocenyl-dithiol ligand. By changing from a monodentate to a bidentate ligand for surface functionalization, the hope was to improve the stability and rigidity of the cluster complex formed and thus single crystal formation.

A freshly prepared coordination polymer (**5**) was solubilized with dppp in CH_2Cl_2. At first the ideal ratio of $S(SiMe_3)_2$ to **5** to yield a silver sulfide core was unknown so using 1 equiv. of $S(SiMe_3)_2$ to **5** was attempted. After a few days, non-crystalline black materials formed. This suggested that the excess of $S(SiMe_3)_2$ may lead to Ag_2S. A smaller amount of $S(SiMe_3)_2$, only 0.1 equiv. to **5**, was introduced in a new reaction. The decreased amount of $S(SiMe_3)_2$ led to a much slower reaction, with no significant color change observed after 3 days. However, 0.3 equiv. of $S(SiMe_3)_2$ to **5** generated block shaped single crystals of $[Ag_{74}S_{19}(dppp)_6(fc(C\{O\}OCH_2CH_2S)_2)_{18}]$ (**9**). (Scheme 3.1)

$[fc(C\{O\}OCH_2CH_2SAg)_2]_n$ + 2 dppp + 0.3 $S(SiMe_3)_2$ $\longrightarrow$ $[Ag_{74}S_{19}(dppp)_6(fc(C\{O\}OCH_2CH_2S)_2)_{18}]$ + ...
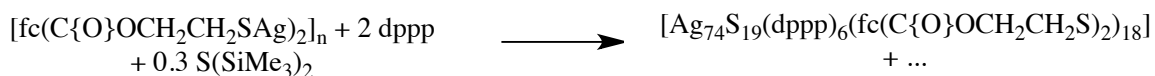
Scheme 3.1 Synthesis of $[Ag_{74}S_{19}(dppp)_6(fc(C\{O\}OCH_2CH_2S)_2)_{18}]$ (**9**)

It was expected that the reagent $fc(C\{O\}OCH_2CH_2SSiMe_3)_2$ (**6**) would have similar reactivity to that previously reported for the monodentate analogue $FcC\{O\}OCH_2CH_2SSiMe_3$, which had been used in the formation of the small ferrocenyl decorated cluster $[Ag_{14}(PPh_3)_6S(SCH_2CH_2O\{O\}CFc)_{12}]$.[6] Thus reactions shown in Scheme 3.3 were attempted. However, despite numerous attempts with different solvents and counter solvent combinations, no single crystals were able to be isolated.

$$fc(C\{O\}OCH_2CH_2SSiMe_3)_2 + 2\ dppp + 2\ AgOAc \longrightarrow$$
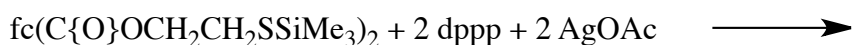
Scheme 3.2 Reactions of $fc(C\{O\}OCH_2CH_2SSiMe_3)_2$ (**6**)

3.4.2 Structural Characterization of $[Ag_{74}S_{19}(dppp)_6(fc(C\{O\}OCH_2CH_2S)_2)_{18}]$ (9)

Cluster **9** was structurally characterized by X-ray crystallography. The molecular structure of **9** is shown in Figure 3.1, which was completely solved and refined in the rhombohedral group $R\bar{3}$ with 3 molecules in the unit cell. All Ag, S, P and (non disordered) Fe atoms were refined anisotropically. All C and O atoms were refined isotropically. Six ferrocenyl units among the eighteen are disordered. A two-site disorder for the ferrocenyl dithiolate ligand "Fe1" was satisfactorily modelled with 50:50 occupancy. For clarity, the disorder hasn't been shown in Figure 3.1.

The cluster 9 resides about a crystallographic $\bar{3}$ site on which resides the central sulfide ion. Figure 3.2, Figure 3.3 and Figure 3.4 display differing representations of the molecular structure of $[Ag_{74}S_{19}(dppp)_6(fc(C\{O\}OCH_2CH_2S)_2)_{18}]$ (**9**). The $Ag_{74}S_{55}$ core ($\sim1.7 \times 1.5 \times 1.4\ nm^3$) of the structure can be described as nearly spherical, consisting of seventy-four silver atoms bonded to nineteen sulfide (S^{2-}) and thirty-six thiolate centers (each $fc(C\{O\}OCH_2CH_2S)_2{}^{2-}$) will provide two). The central sulfide in the core adopts a μ_8-bridging coordination model while the other 18 sulfides form either μ_6 or μ_7 bridges to silver atoms. Thirteen of the S^{2-} are arranged in a (non-bonded) icosahedral arrangement whereas the 6 additional S^{2-} are closer to the cluster surface. The surface thiolates form μ_2,

μ_3, or μ_4 bridges to silver atoms. The Ag (I) adopt three kinds of geometries: a distorted linear one, a trigonal planar one or distorted tetrahedral. The Ag-S bond lengths for **9** range between 2.372 (7) - 2.968 (7) Å, which are in the similar scale compared with the reported, similar sized cluster $[Ag_{70}S_{16}(SPh)_{34}(PhCO_2)_4(triphos)_4]$ (triphos = 1,1,1-tris{(disphenylphosphino)methyl}ethane),[13] whose Ag-S bond lengths range between 2.370 (4) - 2.927 (4) Å, but larger than those of the ferrocenyl analogue $[Ag_{48}S_6(SCH_2Fc)_{36}]$ (Fc = $(\eta^5\text{-}C_5H_5)Fe(\eta^5\text{-}C_5H_4)$) (2.144 (8) − 2.684 (5) Å).[5] Ag- Ag bond lengths measured for cluster **9** range from 2.901 (3) to 3.374 (3) Å. From the Ag-Ag bond lengths it can be concluded that there are no obvious Ag-Ag interactions.[14] This can be supported by the fact that all the silver atoms in cluster **9** can be assigned the formal oxidation state as +1, consistent with the formula $[Ag_{74}S_{19}(dppp)_6(fc(C\{O\}OCH_2CH_2S)_2)_{18}]$ (**9**) as a neutral compound. The six dppp ligands can be described as being at the corners of an octahedron if each P∩P is considered as occupying one vertex position. These, along with the eighteen surface bidentate ferrocenyl dithiolate ligands limit the growth of the cluster core to bulk Ag_2S. From the space filling diagram of **9** (Figure 3.3) it can be observed that the cluster core is perfectly protected by the dppp and ferrocenyl dithiolate ligands, which can be a reasonable explanation for the stability of **9** in solution and the solid state. It is worth mentioning that this is the largest cluster that has been structurally characterized so far that has both a high-nuclearity core and a ferrocene rich surface. The overall dimensions of the cluster (including ferrocenyl shell) are ~ 3.1 x 3.0 x 3.0 nm^3. This synthesis suggests that by applying different selections of phosphine ligands, it is possible to make a series of high-nuclearity clusters with ferrocene rich surfaces.
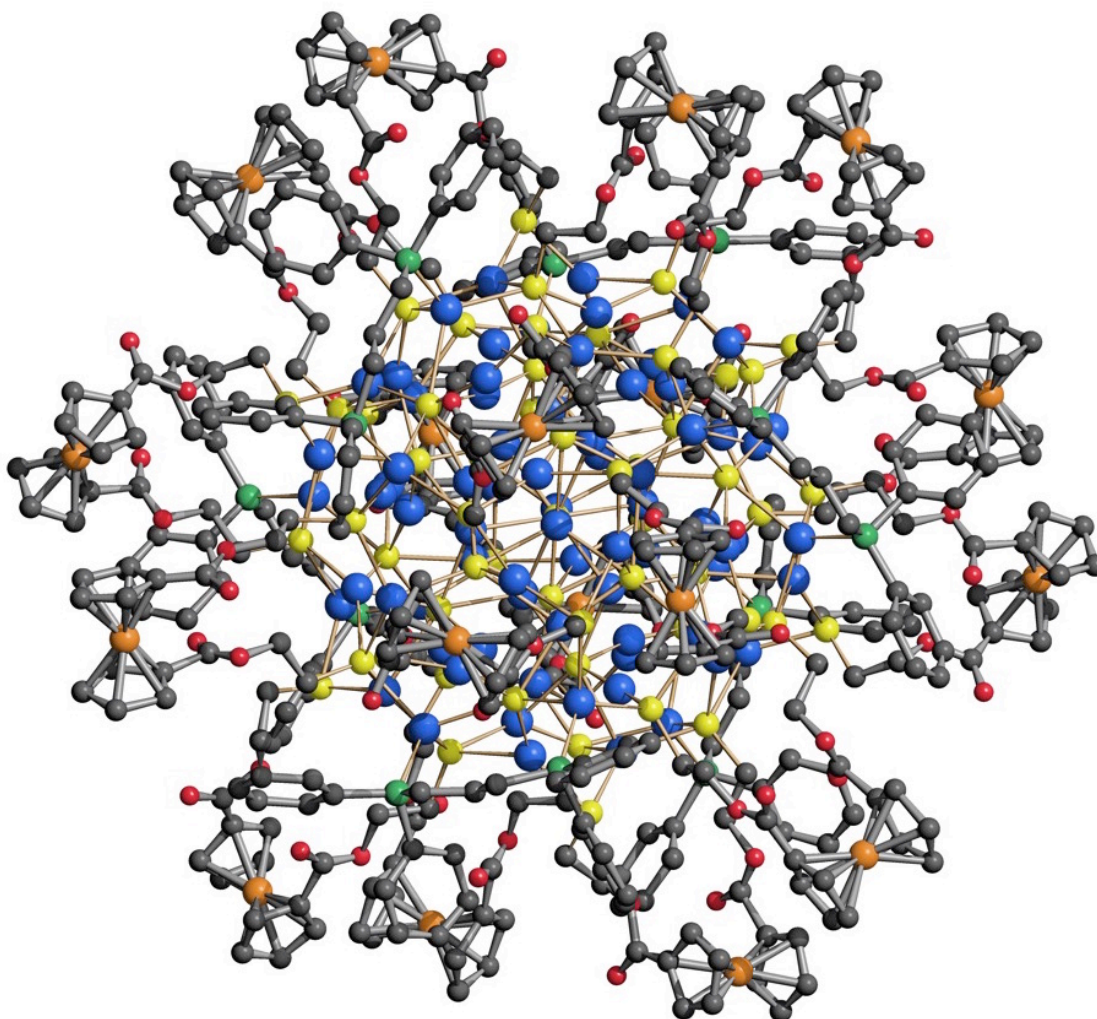
Figure 3.1 Ball and stick diagram of the molecular structure of $[Ag_{74}S_{19}(dppp)_6(fc(C\{O\}OCH_2CH_2S)_2)_{18}]$ (**9**). Hydrogen atoms have been omitted clarity. Ag blue, S yellow, P green, O red, Fe orange, C grey.

Figure 3.2 Ball and stick diagram of the $Ag_{74}S_{55}$ core of $[Ag_{74}S_{19}(dppp)_6(fc(C\{O\}OCH_2CH_2S)_2)_{18}]$ (**9**). Ag blue, S yellow.
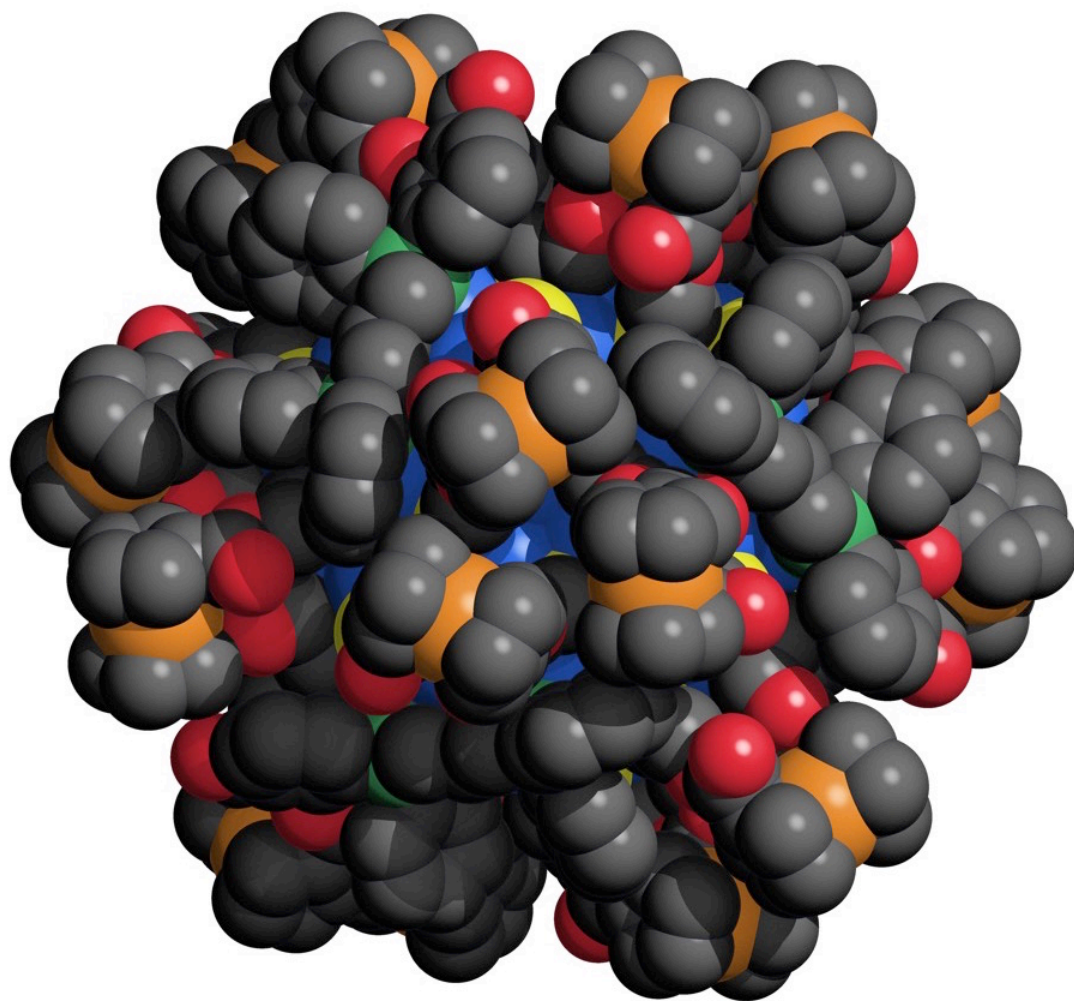
Figure 3.3 Space filling diagram of the molecular structure of [Ag$_{74}$S$_{19}$(dppp)$_6$(fc(C{O}OCH$_2$CH$_2$S)$_2$)$_{18}$] (**9**). Hydrogen atoms have been omitted for clarity. Ag blue, S yellow, P green, O red, Fe orange, C grey.
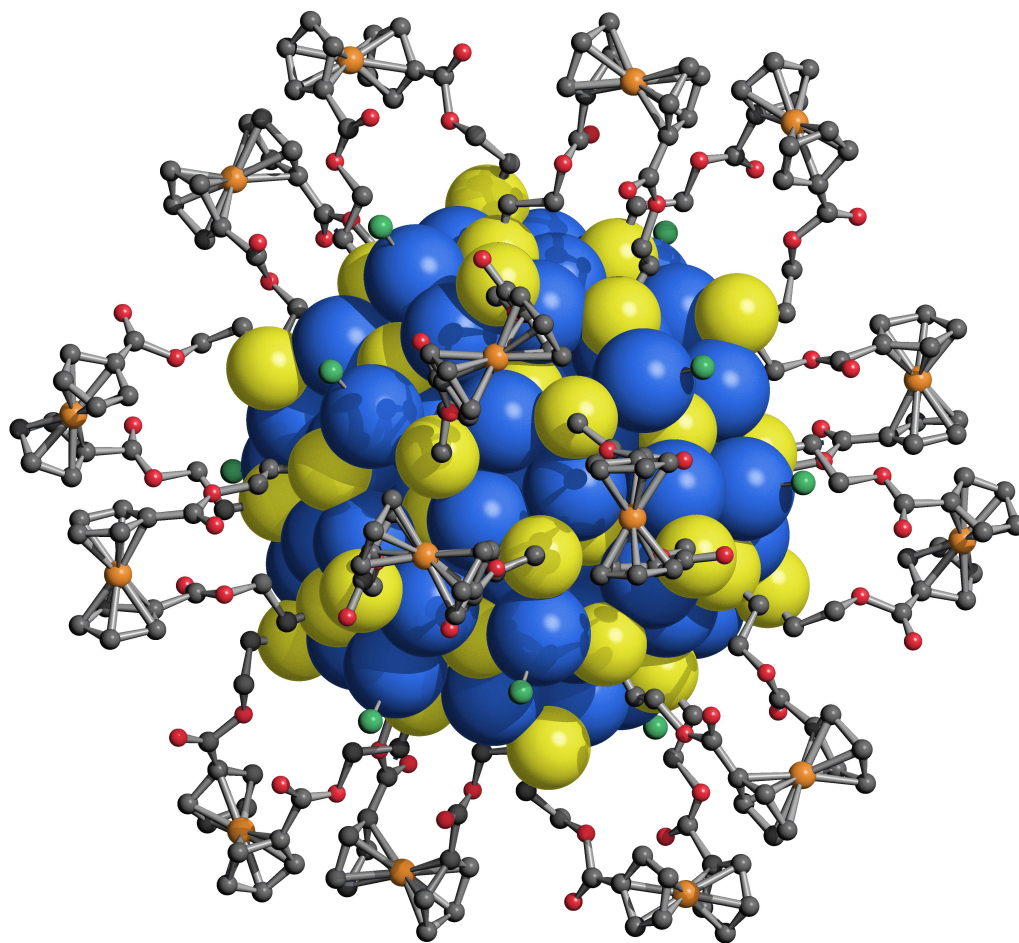
Figure 3.4 Space filling diagram of the $Ag_{74}S_{55}$ core with carbon atoms of dppp omitted to emphasize the distribution of ferrocenyl dithiolate ligands in $[Ag_{74}S_{19}(dppp)_6(fc(C\{O\}OCH_2CH_2S)_2)_{18}]$ (**9**). Hydrogen atoms have been omitted. Ag blue, S yellow, P green, O red, Fe orange, C grey.

3.4.3 Electrochemistry of fc(C{O}OCH$_2$CH$_2$Br)$_2$ (1) and [Ag$_{74}$S$_{19}$(dppp)$_6$(fc(C{O}OCH$_2$CH$_2$S)$_2$)$_{18}$] (9)

3.4.3.1 Cyclic Voltammetry

Cyclic voltammograms of fc(C{O}OCH$_2$CH$_2$Br)$_2$ (1) and [Ag$_{74}$S$_{19}$(dppp)$_6$(fc(C{O}OCH$_2$CH$_2$S)$_2$)$_{18}$] (9) were obtained using a BAS 100 electrochemical workstation using a 3-electrode system, with a platinum flag counter electrode, a Ag/AgCl reference electrode and a glassy carbon working electrode. NBu$_4$PF$_6$ (0.1 M) in CH$_2$Cl$_2$ was used as the supporting electrolyte. A 1 mM solution of 1 was prepared in CH$_2$Cl$_2$ for the measurements but the limited solubility of 9 prevented the preparation of a similarly concentrated solution. The slight solubility of 9 in CH$_2$Cl$_2$ was such that a solution was prepared with 1 mg of 9 dissolved in 20 mL of CH$_2$Cl$_2$, after stirring in the dark for one week some solid was left undissolved, so the accurate concentration for 9 couldn't be determined, but was less than 0.003 mM.

Cyclic voltammetry was used to investigate the redox activity of the iron centers in 1 and 9, and the cyclic voltammograms of 1 and 9 are shown in Figure 3.5 and Figure 3.6, respectively.

For 1, a single reversible oxidation wave was observed for scan rates ranging from 300 mV/s to 50 mV/s. This reversible peak is assigned to the oxidation and reduction of the ferrocene moiety in the molecule of 1. It shows an oxidation peak at $E_{1/2}$ ($E_{1/2}$ = (E_{pa} + E_{pc})/2) of 980 mV with ΔE = | E_{pa} - E_{pc}| = 99 mV at a scan rate of 100 mV/s and the i_{pa}/i_{pc} value for this peak is 1.0 (shown in Figure 3.5). For 9, only one quasi-reversible redox wave was observed at the scan rates range from 300 mV/s to 50 mV/s, whose peak is broader than that of 1, which suggests that the ferrocene moieties at the surface of 9 are oxidized at a potential similar to each other. The $E_{1/2}$ ($E_{1/2}$ = (E_{pa} + E_{pc})/2) was 949 mV with ΔE = | E_{pa} - E_{pc}| = 168 mV at a scan rate of 100 mV/s and the i_{pa}/i_{pc} value for this peak is 1.1 (shown in Figure 3.6).

For both 1 and 9, the ΔE values suggest that the oxidation of the ferrocene moieties is electrochemically irreversible because the theoretical ΔE for a one-electron oxidation

process is 59 mV.[15] However, the shape of voltammograms shows that the oxidation of both the ferrocenyl ligands and the cluster are chemically reversible. Comparing the CV data of **9** with that of its analogue, $[Ag_{36}S_9(SCH_2CH_2O\{O\}CFc)_{18}(PPh_3)_3]$,[16] it suggested limited absorption of **9** to the electrode. The single wave of the CV of **9** makes it an ideal candidate for ion or molecular recognition.
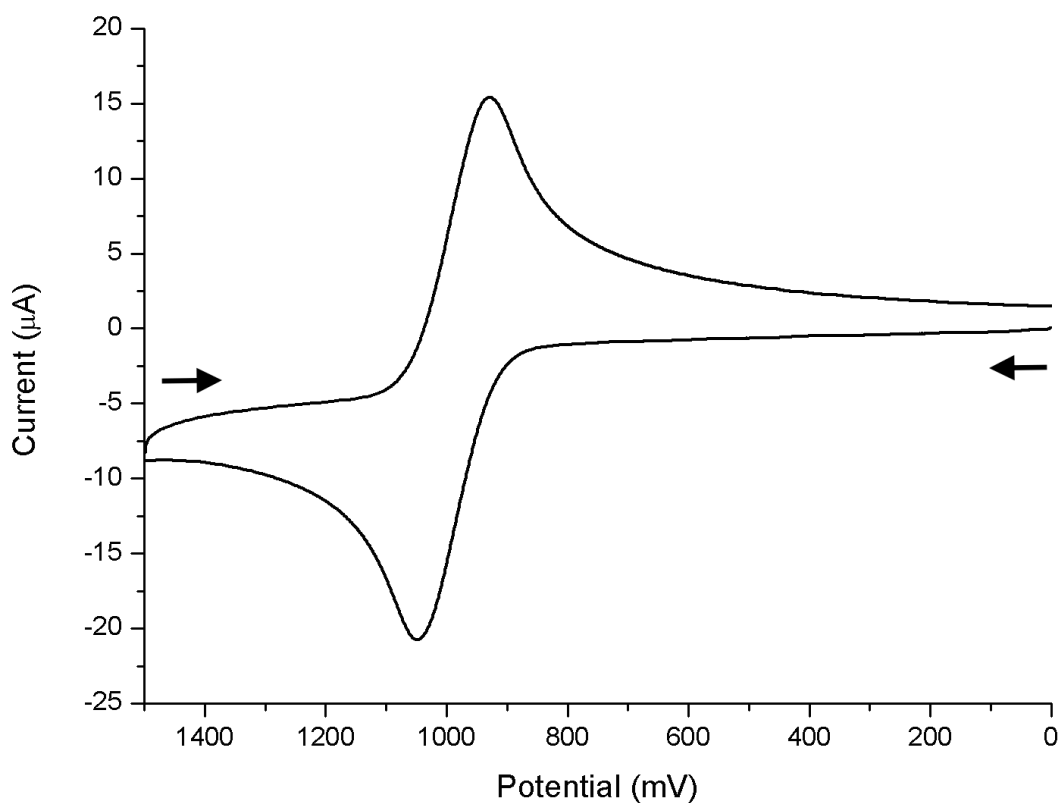
Figure 3.5 Cyclic voltammogram of **1** (1 mM) using glassy carbon working electrode in dry CH_2Cl_2 and $[NBu_4][PF_6]$ (0.1 M) as supporting electrolyte at a scan rate of 100 mV/s. Peak potentials are referenced to Ag/AgCl.
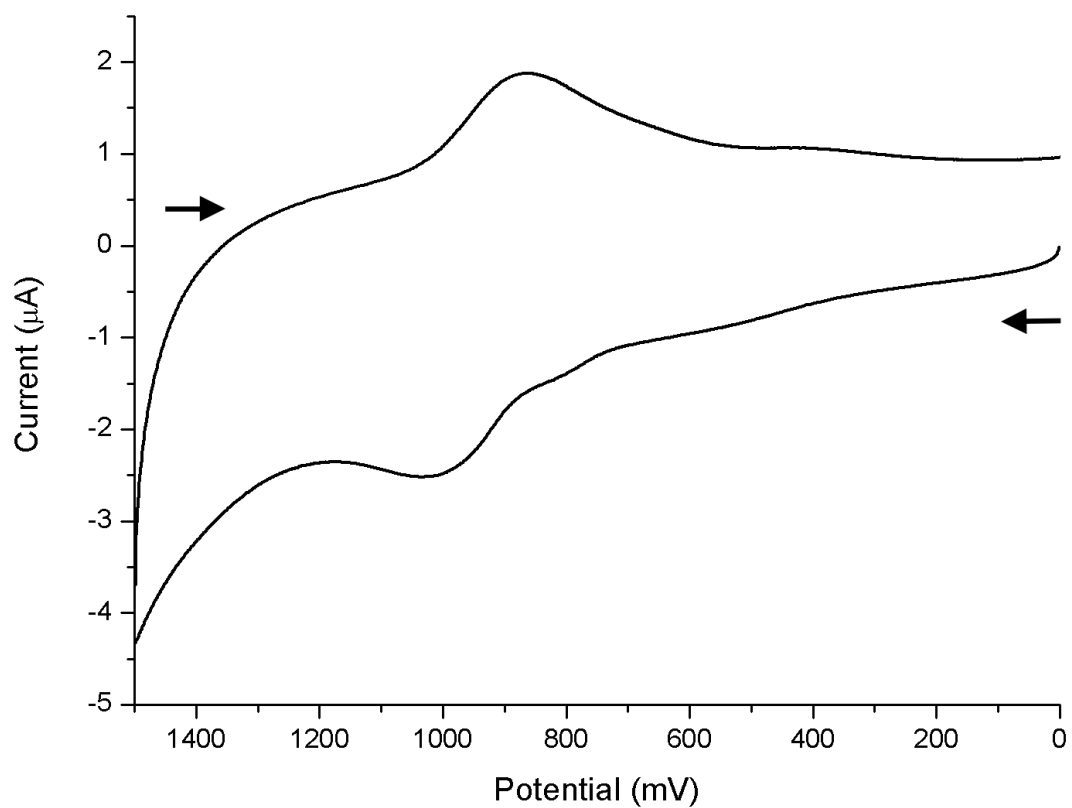
Figure 3.6 Cyclic voltammogram of **9** (<0.003 mM) using glassy carbon working electrode in dry CH_2Cl_2 and $[NBu_4][PF_6]$ (0.1 M) as supporting electrolyte at a scan rate of 100 mV/s. Peak potentials are referenced to Ag/AgCl.

3.4.3.2 Preliminary Anion Sensing Studies

In this study, a platinum working electrode was chosen for **1** because a smallest ΔE was shown compared with that of either a gold or a glassy carbon working electrode when other conditions were unchanged; a glassy carbon working electrode was chosen for **9** because the solubility of **9** was very low and the larger surface interface of glassy carbon working electrode made it the only one to receive a significant signal.
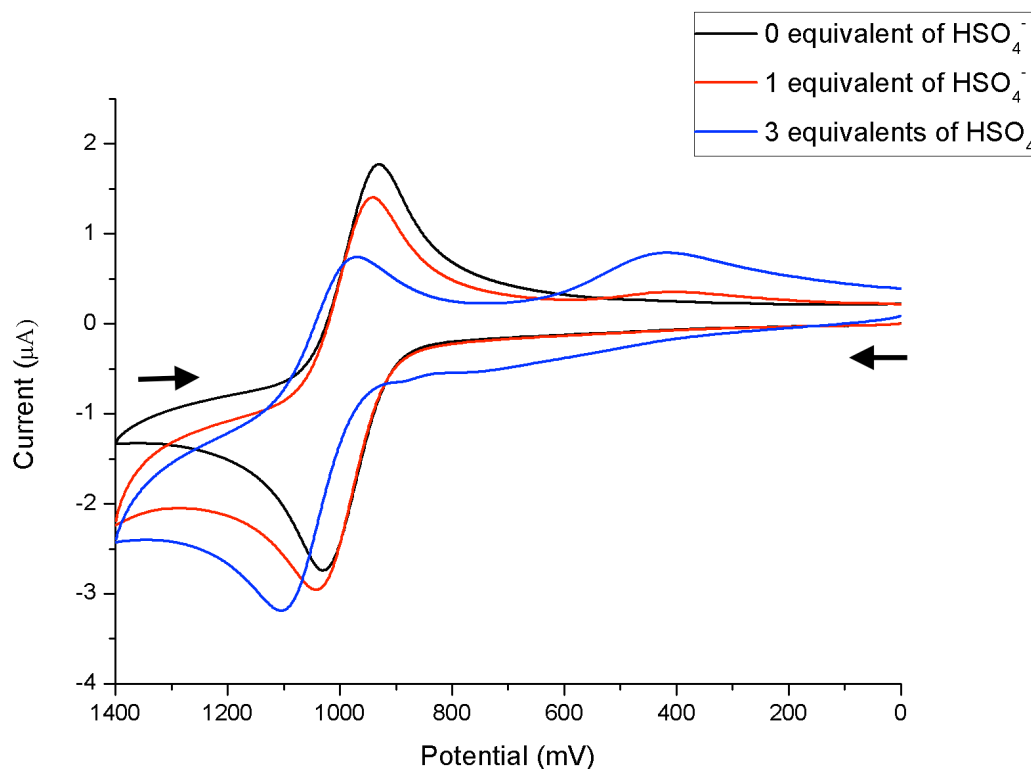
Figure 3.7 Cyclic voltammogram of **1** (1 mM) using Pt working electrode in dry CH_2Cl_2 and $[NBu_4][PF_6]$ (0.1 M) as supporting electrolyte at a scan rate of 100 mV/s, upon addition of different ratios of $[NBu_4][HSO_4]$. Peak potentials are referenced to Ag/AgCl.

The addition of [NBu$_4$][HSO$_4$] to a solution of ferrocenyl complex fc(C{O}OCH$_2$CH$_2$Br)$_2$ (**1**) in CH$_2$Cl$_2$ showed no change in the potential of the CV curve upon addition of less than 1 equivalent. At 1 equivalent, a small secondary oxidation peak was observed at a more negative potential, while continued addition of [NBu$_4$][HSO$_4$] resulted in the secondary peak increasing in intensity. This suggests that an interaction occurred upon addition of [NBu$_4$][HSO$_4$] into the solution of **1**, which made the substituents on the C$_5$ rings in **1** less electron withdrawing, leading to the Fe (II) center being easier to be oxidized. The nature of this interaction is not at all clear.

The addition of [NBu$_4$][HSO$_4$] to a solution of cluster **9** in CH$_2$Cl$_2$ (<0.003 mmol) did not result in any perturbation of the cyclic voltammogram.

3.4.4 UV-Vis Absorption Spectroscopy

The solution electronic absorption spectrum of cluster **9** is presented in Figure 3.8. For the diethylferrocenylcarboxylate dithiol **4**, the spectrum shows three characteristic maxima: a broad maximum at 307 nm, a shoulder at 345 nm, and a broad absorption centered at 450 nm (shown in Figure 2.9); for cluster **9**, however, the characteristic absorption maxima for [fc(C{O}OCH$_2$CH$_2$S)$_2$$^{2-}$] are not observed but a rather featureless absorption profile, with an absorption onset greater than 800 nm. This profile is typical for the absorption spectra of larger silver-sulfide clusters, which are often featureless.[17] The electronic transition in this silver-sulfide core can be assigned to a 3p(S)➔5s(Ag) ligand to metal charge transfer (LMCT).[18, 19] The luminescence that has been observed for silver chalcogenolates[20] is not observed for cluster **9**. This is not unexpected due to the surface modification of **9** with ferrocenyl ligands. Previous report have shown that the incorporation of ferrocenyl ligands onto CdSe or CdSe/ZnS quantum dots to be capable of quenching their fluorescence.[21, 22]
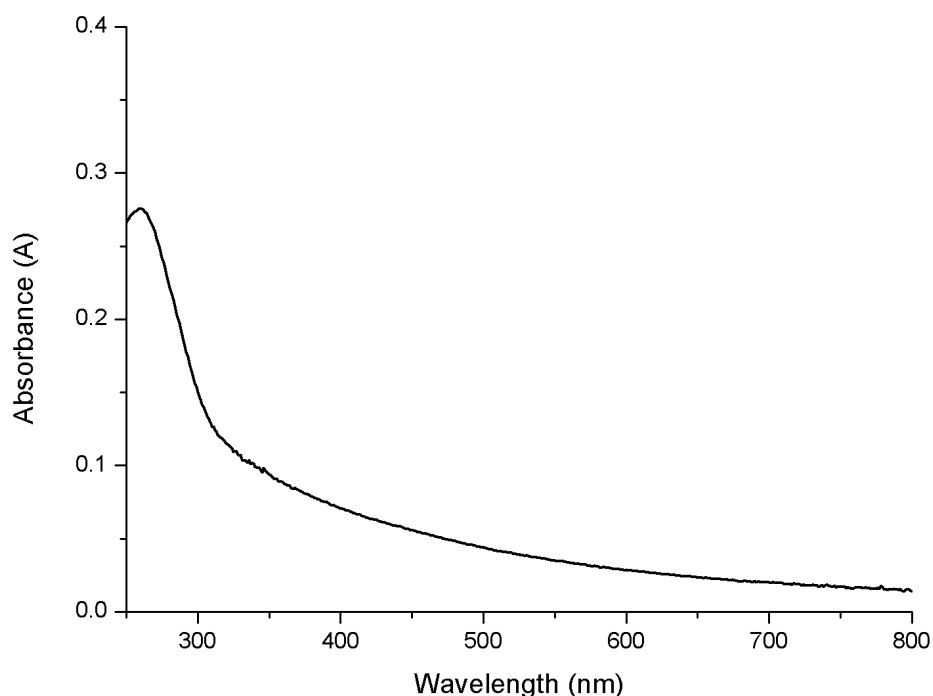
Figure 3.8 UV-Vis absorption spectrum of $[Ag_{74}S_{19}(dppp)_6(fc(C\{O\}OCH_2CH_2S)_2)_{18}]$ (**9**) at a concentration of approximately 0.003 mM (~1 mg in 20 mL CH_2Cl_2).

3.5 Conclusions

The use of bidentate ferrocenylester dithiolate coordination polymer in the assembly of the silver sulfide cluster $[Ag_{74}S_{19}(dppp)_6(fc(C\{O\}OCH_2CH_2S)_2)_{18}]$ (**9**) presents a new way to access these large high-nuclearity molecules with different functionalities on their surfaces. CV measurements of $[Ag_{74}S_{19}(dppp)_6(fc(C\{O\}OCH_2CH_2S)_2)_{18}]$ (**9**) display a quasi reversible single redox wave, which makes it a good candidate for molecule recognition; although preliminary ion sensing studies showed that **9** was not sensitive to HSO_4^-, it is still potential for recognize other species as all the redox centers are stable on the surface of **9**.

3.6 References for Chapter 3

1. Nguyen, P.; Elipe, P. G.; Manners, I. *Chem. Rev.* **1999**, *99*, 1515.

2. Beer, P. D.; Gale, P. A. *Angew. Chem. Int. Ed.* **2001**, *40*, 486.

3. Astruc, D.; Daniel, M-C.; Ruiz, J. *Chem. Commun.* **2004**, 2637.

4. Nitschke, C.; Wallbank, A. I.; Fenske, D.; Corrigan, J. F. *J. Cluster Sci.* **2007**, *18*, 131.

5. Ahmar, S.; MacDonald, D. G.; Vijayaratnam, N.; Battista, T. L.; Workentin, M. S.; Corrigan, J. F. *Angew. Chem. Int. Ed.* **2010**, *49*, 4422.

6. MacDonald, D. G.; Eichhöfer, A.; Campana, C. F.; Corrigan, J. F. *Chem. Eur. J.* **2011**, *17*, 5890.

7. a) Fenske, D.; Ohmer, J.; Hachgenei, J.; Nerzweiler, K. *Angew. Chem. Int. Ed. Engl.* **1988**, *27*, 1277. b) Degroot, M. W.; Corrigan, J. F. *Comprehensive Coordination Chemistry II*, eds. Fujia, M.; Powell, A.; Creutz, C., Pergamon: Oxford, U.K., **2004**, *7*, 57. c) Fenske, D. *Clusters and Colloids, From Theory to Applications*; ed. Schmid, G.; VCH: Weinheim, **1994**, 212. d) Dehnen, S.; Eichhöfer, A.; Fenske, D. *Eur. J. Inorg. Chem.* **2002**, 279.

8. Fenske, D.; Anson, A. E.; Eichhöfer, A.; Fuhr, O.; Ingendoh, A.; Persau, C.; Richert, C. *Angew. Chem. Int. Ed.* **2005**, *44*, 5242.

9. Anson, C.E.; Eichhöfer, A.; Issac, I.; Fenske, D.; Fuhr, O.; Sevillano, P.; Persau, C.; Stalke, D.; Zhang, J. *Angew. Chem. Int. Ed.* **2008**, *47*, 1326.

10. MacDonald, D. G.; Kübel, C.; Corrigan, J. F. *Inorg. Chem.* **2011**, *50*, 3252.

11. Taher, D.; Wallbank, A. I.; Turner, E. A.; Cuthbert, H. L.; Corrigan, J. F. *Eur. J. Inorg. Chem.* **2006**, 4616.

12. Sheldrick, G. M. *Acta Cryst.* **2008**, *A64*, 112.

13. Wang, X.; Langetepe, T.; Persau, C.; Kang, B.; Sheldrick, G. M.; Fenske, D. *Angew. Chem. Int. Ed.* **2002**, *41*, 3818.

14. Tang, K.; Xie, X.; Zhang, Y.; Zhao, X.; Jin, X. *Chem. Commun.* **2002**, 1024.

15. Kissinger, P. T.; Heineman, W. R. *J. Chem. Educ.* **1983**, *60*, 702.

16. MacDonald, D. G. Ph. D. Thesis, University of Western Ontario, 2010.

17. Schaaff, T. G.; Rodinone, A. J. *J. Phys. Chem. B* **2003,** *107,* 10146.

18. Brühwiler, D.; Seifert, R.; Calzaferri, G. *J. Phys. Chem. B.* **1999**, *103*, 6397.

19. Brühwiler, D.; Leiggener, C.; Stephan, G.; Calzaferri, G. *J. Phys. Chem. B.* **2002**, *106*, 3770.

20. Li, G.; Lei, Z.; Wang, Q. *J. Am. Chem. Soc.* **2010**, *132*, 17678.

21. Palaniappan, K.; Hackney, S. A.; Liu, J. *Chem. Commun.* **2004**, 2074.

22. Mulrooney, R. C.; Singh, N.; Kaur, N.; Callan, J. F. *Chem. Commun.* **2009**, 686.

Chapter 4
General Conclusions and Outlook

4.1 Summary

The isolation and structural characterization of metal-chalcogen clusters have given researchers the opportunities to inspect the unique properties arising from decreasing size of the corresponding bulk material.[1] Silylated reagents have proven to offer a powerful route to synthesize metal chalcogen clusters with a large series of them having been synthesized and structurally characterized.[2,3,4,5] Recently, another synthetic route for silver chalcogen clusters was reported by Fenske and co-workers by applying silver thiolate coordination polymers (AgSR) as precursors.[6,7] This yielded the largest structurally characterized silver sulfide cluster reported to date, $[Ag_{490}S_{188}(StC_5H_{11})_{114}]$.[7]

In this thesis, two new bidentate ferrocenyl based dithiol ligands were successfully synthesized. Bidentate ferrocenyl chalcogen ligands were targeted due to the fact that they have two points of ligation to the cluster cores, which may help increase the stability and rigidity of the corresponding clusters compared to the monodentate analog.[8] The targeted ligands were designed to have either an ester or amide functionality because that may help the ligands with ion sensing (for example, through the formation of H-bond with analytes).[9,10] $fc(C\{O\}OCH_2CH_2Br)_2$ **1** was synthesized using an ester coupling reaction. 1,1'-ferrocenyl dicarboxylic acid was first transferred to 1,1'-ferrocenyl dicarbonyl chloride and then coupled with 2-bromoalcohol with the presence of triethylamine to give out $fc(C\{O\}OCH_2CH_2Br)_2$ **1**. $fc(C\{O\}OCH_2CH_2Br)COOH$ **2** and $(fc(C\{O\}O\{O\}C))_2$ **3** were also isolated from this reaction as byproducts due to partial hydrolysis of 1,1'-ferrocenyl dicarbonyl chloride. Bidentate ethylferrocenylcarboxylate dithiol $fc(C\{O\}OCH_2CH_2SH)_2$ **4** was prepared using $fc(C\{O\}OCH_2CH_2Br)_2$ **1** as precursor in a reaction with $S(SiMe_3)_2$ and tetrabutylammonium fluoride (TBAF). $fc(C\{O\}NHCH_2CH_2Cl)_2$ **7** was synthesized using an amide coupling reaction. Starting directly from 1,1'-ferrocenyl dicarboxylic acid with 2-chloroethyl amine, 1-(3-dimethylaminopropyl)-3-ethylcarbodiimide hydrochloride (EDC) was used as amide coupling reagents to promote the reaction and $fc(C\{O\}NHCH_2CH_2Cl)_2$ **7** was yielded in

high purity. The preparation of ligand fc(C{O}NHCH$_2$CH$_2$SH)$_2$ **8** was a little challenging due to its sensitivity. Using fc(C{O}NHCH$_2$CH$_2$Cl)$_2$ **7** as precursor with S(SiMe$_3$)$_2$ and TBAF, fc(C{O}NHCH$_2$CH$_2$SH)$_2$ **8** could be prepared with care.

The coordination polymer [fc(C{O}OCH$_2$CH$_2$SAg)$_2$] **5** was prepared by simply adding CF$_3$SO$_3$Ag and NEt$_3$ into a solution of fc(C{O}OCH$_2$CH$_2$SH)$_2$ **4**. The use of **5** in nanocluster formation was successful, ending with X-ray characterizable single crystals of [Ag$_{74}$S$_{19}$(dppp)$_6$(fc(C{O}OCH$_2$CH$_2$S)$_2$)$_{18}$] **(9)**. The cluster core exhibits an overall spherical shape. Typical bridging models for sulfur were observed for the cluster core Ag$_{74}$S$_{55}$, as μ_2, μ_3 and μ_4 for the thiolate and μ_6, μ_7 and μ_8 for the sulfide. With a core diameter of ~1.9 nm and overall diameter of ~3.1 nm, **9** is the largest cluster with a high-nuclearity core and ferrocene rich surface that has been structurally characterized to date. The electrochemistry of **9** revealed a single redox wave that is comparable with that observed for fc(C{O}OCH$_2$CH$_2$Br)$_2$ (**1**), suggesting the ferrocenyl units oxidized at a similar potential.

The synthesis of **4** and **7** and the reactivity of **5** towards the formation of [Ag$_{74}$S$_{19}$(dppp)$_6$(fc(C{O}OCH$_2$CH$_2$S)$_2$)$_{18}$] **(9)** have been discussed in this thesis. The ester functionality was targeted due to its ease of handling while the amide functionality was also developed because it may give the species an oxo-anoin recognition capacity. Future work using bidentate ferrocenyl chalcogen reagents should be pursued, as the reactivity of the coordination polymer **5** is still to be tested with different tertiary phosphine ligands in the formation of a series of clusters. The bidentate ferrocenyl amide functionalized dithiol **7** should be also used with care to transfer into a Ag (I) coordination polymer, and targeted for the formation of clusters which could serve in ion sensing studies.

4.2 References for Chapter 4

1. Soloviev, V. N.; Eichhöfer, A.; Fenske, D.; Banin, U. *J. Am. Chem. Soc.* **2001**, *123*, 2354.

2. Fenske, D.; Ohmer, J.; Hachgenei, J. *Angew. Chem. Int. Ed. Engl.* **1985**, *24*, 993.

3. Fenske, D.; Langetepe, T.; Kappes, M. M.; Hampe, O.; Weis, P. *Angew. Chem. Int. Ed.* **2000**, *39*, 1857.

4. Nitschke, C.; Wallbank, A. I.; Fenske, D.; Corrigan, J. F. *J. Cluster Sci.* **2007**, *18*, 131.

5. Chitsaz, S.; Fenske, D.; Fuhr, O. *Angew. Chem. Int. Ed.* **2006**, *45*, 8055.

6. Fenske, D.; Anson, A. E.; Eichhöfer, A.; Fuhr, O.; Ingendoh, A.; Persau, C.; Richert, C. *Angew. Chem. Int. Ed.* **2005**, *44*, 5242.

7. Anson, C.E.; Eichhöfer, A.; Issac, I.; Fenske, D.; Fuhr, O.; Sevillano, P.; Persau, C.; Stalke, D.; Zhang, J. *Angew. Chem. Int. Ed.* **2008**, *47*, 1326.

8. MacDonald, D. G.; Kübel, C.; Corrigan, J. F. *Inorg. Chem.* **2011**, *50*, 3252.

9. Beer, P. D. *Chem. Commun.* **1996**, 689.

10. Beer, P. D.; Gale, P. A. *Angew. Chem. Int. Ed.* **2001**, *40*, 486.

APPENDIX 1.

Crystal data and structure refinement for fc(C{O}OCH$_2$CH$_2$Br)$_2$ (**1**)

Formula	C$_{16}$H$_{16}$Br$_2$FeO$_4$
Formula Weight (*g/mol*)	487.96
Crystal Dimensions (*mm*)	0.235 × 0.235 × 0.171
Crystal Color and Habit	orange needle
Crystal System	monoclinic
Space Group	*P* 2$_1$
Temperature, K	150(2)
a, Å	5.7602(10)
b, Å	21.827(4)
c, Å	6.6550(13)
α,°	90
β,°	101.322(5)
γ,°	90
V, Å^3	820.4(3)
Number of reflections to determine final unit cell	9746
Min and Max 2θ for cell determination, °	6.24, 66.64
Z	2
F(000)	480
ρ (*g/cm*)	1.975
λ, Å, (MoKα)	0.71073
μ, (*cm^{-1}*)	5.805
Diffractometer Type	Bruker APEX-II CCD
Scan Type(s)	and scans
Max 2θ for data collection, °	70.928
Measured fraction of data	0.999
Number of reflections measured	18885
Unique reflections measured	5687
R$_{merge}$	0.0259
Number of reflections included in refinement	5687
Cut off Threshold Expression	I > 2sigma(I)
Structure refined using	full matrix least-squares using F^2
Weighting Scheme	w=1/[sigma^2(Fo^2)+(0.0441P)^2+0.1543P] where P=(Fo^2+2Fc^2)/3
Number of parameters in least-squares	209
R$_1$	0.0342
wR$_2$	0.0782
R$_1$ (all data)	0.0413
wR$_2$ (all data)	0.0803
GOF	1.036
Maximum shift/error	0.001
Min & Max peak heights on final ΔF Map (*e$^-$/Å*)	-0.743, 2.074

Atomic Coordinates for fc(C{O}OCH$_2$CH$_2$Br)$_2$ (**1**)

Atom	x	y	z	U$_{iso/equiv}$
Fe1	0.76186(8)	0.75058(2)	0.47370(8)	0.01379(10)
Br1	1.31635(8)	0.57582(2)	0.84437(7)	0.02962(11)
Br2	1.32821(7)	0.92927(2)	1.28649(6)	0.02696(10)
C1	0.8529(6)	0.69669(18)	0.2538(6)	0.0163(7)
C2	0.6103(7)	0.71597(18)	0.1910(6)	0.0178(7)
C3	0.6129(8)	0.78081(19)	0.1835(6)	0.0195(7)
C4	0.8504(7)	0.80196(19)	0.2405(6)	0.0200(7)
C5	1.0007(6)	0.7496(2)	0.2858(5)	0.0170(6)
C6	0.8062(6)	0.80343(17)	0.7302(6)	0.0147(6)
C7	0.5633(7)	0.78544(18)	0.6681(6)	0.0170(7)
C8	0.5530(7)	0.72069(18)	0.6714(6)	0.0174(7)
C9	0.7887(7)	0.69804(19)	0.7346(6)	0.0186(7)
C10	0.9467(6)	0.74875(19)	0.7711(5)	0.0169(6)
C11	0.9215(6)	0.63233(18)	0.2879(6)	0.0172(7)
O1	0.7866(5)	0.58914(13)	0.2481(5)	0.0246(6)
O2	1.1545(5)	0.62583(13)	0.3676(4)	0.0188(5)
C12	1.2373(7)	0.56389(19)	0.4051(7)	0.0222(8)
C13	1.1629(7)	0.53596(19)	0.5898(7)	0.0227(8)
C14	0.8883(6)	0.86688(17)	0.7460(6)	0.0168(7)
O3	0.7642(5)	0.91120(14)	0.6992(5)	0.0237(6)
O4	1.1243(5)	0.87058(13)	0.8252(5)	0.0202(6)
C15	1.2215(6)	0.9324(2)	0.8475(6)	0.0211(7)
C16	1.1660(7)	0.96527(19)	1.0277(6)	0.0224(8)
H2	0.4750	0.6902	0.1605	0.021
H3	0.4773	0.8062	0.1463	0.023
H4	0.9003	0.8435	0.2473	0.024
H5	1.1680	0.7500	0.3291	0.020
H7	0.4321	0.8123	0.6312	0.020
H8	0.4137	0.6965	0.6375	0.021
H9	0.8327	0.6561	0.7498	0.022
H10	1.1139	0.7468	0.8144	0.020
H12A	1.4123	0.5635	0.4258	0.027
H12B	1.1746	0.5386	0.2830	0.027
H13A	1.2037	0.4919	0.5969	0.027
H13B	0.9890	0.5395	0.5747	0.027
H15A	1.1574	0.9561	0.7220	0.025
H15B	1.3955	0.9302	0.8609	0.025
H16A	0.9929	0.9641	1.0216	0.027
H16B	1.2136	1.0087	1.0224	0.027

APPENDIX 2.

Crystal data and structure refinement for fc(C{O}OCH$_2$CH$_2$Br)COOH (**2**)

Formula	C$_{14}$H$_{13}$BrFeO$_4$
Formula Weight (*g/mol*)	381.00
Crystal Dimensions (*mm*)	0.903 × 0.180 × 0.039
Crystal Color and Habit	orange plate
Crystal System	monoclinic
Space Group	*P* 2$_1$/n
Temperature, K	110
a, Å	14.249(5)
b, Å	5.8069(18)
c, Å	17.366(5)
α,°	90
β,°	110.094(14)
γ,°	90
V, Å^3	1349.4(7)
Number of reflections to determine final unit cell	6732
Min and Max 2θ for cell determination, °	5.0, 56.18
Z	4
F(000)	760
ρ (*g/cm*)	1.875
λ, Å, (MoKα)	0.71073
μ, (*cm^{-1}*)	4.087
Diffractometer Type	Bruker Kappa Axis Apex2
Scan Type(s)	phi and omega scans
Max 2θ for data collection, °	58.868
Measured fraction of data	0.998
Number of reflections measured	15445
Unique reflections measured	3282
R$_{merge}$	0.0261
Number of reflections included in refinement	3282
Cut off Threshold Expression	I > 2sigma(I)
Structure refined using	full matrix least-squares using F^2
Weighting Scheme	w=1/[sigma^2(Fo^2)+(0.0297P)^2+3.8124P] where P=(Fo^2+2Fc^2)/3
Number of parameters in least-squares	182
R$_1$	0.0342
wR$_2$	0.0807
R$_1$ (all data)	0.0479
wR$_2$ (all data)	0.0861
GOF	1.041
Maximum shift/error	0.000
Min & Max peak heights on final ΔF Map (*e$^-$/Å*)	-1.160, 0.707

Atomic Coordinates for fc(C{O}OCH$_2$CH$_2$Br)COOH (**2**)

Atom	x	y	z	U$_{iso/equiv}$
Fe1	0.66198(3)	0.23652(6)	0.39782(2)	0.00945(10)
Br1	0.41688(3)	-0.19372(7)	0.14605(2)	0.03614(12)
O1	0.37466(15)	0.1706(4)	0.33536(14)	0.0218(5)
O2	0.44630(14)	-0.1793(3)	0.34025(12)	0.0167(4)
O3	0.93521(15)	0.2801(4)	0.48070(13)	0.0203(5)
O4	0.90253(15)	-0.0686(4)	0.42131(13)	0.0196(4)
C1	0.5422(2)	0.1096(5)	0.42273(16)	0.0123(5)
C2	0.5658(2)	0.3361(5)	0.45573(17)	0.0154(6)
C3	0.6651(2)	0.3321(5)	0.51244(17)	0.0187(6)
C4	0.7031(2)	0.1041(5)	0.51382(17)	0.0172(6)
C5	0.6278(2)	-0.0349(5)	0.45854(16)	0.0146(6)
C6	0.7878(2)	0.2347(5)	0.36891(17)	0.0131(5)
C7	0.7528(2)	0.4666(5)	0.36887(17)	0.0144(6)
C8	0.6551(2)	0.4775(5)	0.30912(17)	0.0146(5)
C9	0.6303(2)	0.2566(5)	0.27257(17)	0.0146(5)
C10	0.7116(2)	0.1056(5)	0.30909(16)	0.0130(5)
C11	0.4457(2)	0.0440(5)	0.36164(17)	0.0134(5)
C12	0.3547(2)	-0.2728(5)	0.28350(19)	0.0192(6)
C13	0.3767(2)	-0.4011(5)	0.21733(18)	0.0204(6)
C14	0.8803(2)	0.1336(5)	0.42570(17)	0.0142(6)
H3	0.9842	0.2105	0.5138	0.030
H2	0.5227	0.4661	0.4422	0.019
H3A	0.7002	0.4589	0.5439	0.022
H4	0.7681	0.0536	0.5464	0.021
H5	0.6332	-0.1936	0.4474	0.017
H7	0.7882	0.5896	0.4024	0.017
H8	0.6136	0.6100	0.2959	0.017
H9	0.5694	0.2168	0.2307	0.018
H10	0.7149	-0.0525	0.2962	0.016
H12A	0.3070	-0.1464	0.2593	0.023
H12B	0.3237	-0.3777	0.3128	0.023
H13A	0.3164	-0.4877	0.1843	0.025
H13B	0.4308	-0.5136	0.2423	0.025

APPENDIX 3.

Crystal data and structure refinement for ((fc(C{O}O{O}C))$_2$) (**3**)

Formula	$C_{24}H_{16}Fe_2O_6$
Formula Weight (*g/mol*)	512.07
Crystal Dimensions (*mm*)	0.155 × .047 × .023
Crystal Color and Habit	orange plate
Crystal System	monoclinic
Space Group	*P* 2$_1$/n
Temperature, K	110
a, Å	6.1724(13)
b, Å	7.7503(18)
c, Å	19.732(6)
a,°	90
b,°	94.628(13)
g,°	90
V, Å^3	940.9(4)
Number of reflections to determine final unit cell	4875
Min and Max 2q for cell determination, °	5.64, 63.1
Z	2
F(000)	520
r (*g/cm*)	1.808
l, Å, (MoKa)	0.71073
m, (*cm^{-1}*)	1.586
Diffractometer Type	Bruker Kappa Axis Apex2
Scan Type(s)	phi and omega scans
Max 2q for data collection, °	63.44
Measured fraction of data	0.997
Number of reflections measured	14188
Unique reflections measured	3166
R$_{merge}$	0.0776
Number of reflections included in refinement	3166
Cut off Threshold Expression	I > 2sigma(I)
Structure refined using	full matrix least-squares using F^2
Weighting Scheme	w=1/[sigma^2(Fo^2)+(0.0545P)^2+0.6785P] where P=(Fo^2+2Fc^2)/3
Number of parameters in least-squares	145
R$_1$	0.0421
wR$_2$	0.0960
R$_1$ (all data)	0.0706
wR$_2$ (all data)	0.1197
GOF	1.015
Maximum shift/error	0.001
Min & Max peak heights on final DF Map (*e$^-$/*Å)	-0.925, 0.796

Atomic Coordinates for ((fc(C{O}O{O}C))$_2$) (**3**)

Atom	x	y	z	$U_{iso/equiv}$
Fe1	0.43327(6)	0.76862(4)	0.13498(2)	0.01638(11)
O1	0.0737(3)	0.7556(3)	-0.02439(11)	0.0284(5)
O2	0.4059(3)	0.8363(2)	-0.05765(9)	0.0198(4)
O3	0.1725(3)	0.8248(3)	-0.15363(10)	0.0239(4)
C12	0.3377(4)	0.8755(3)	-0.12478(13)	0.0186(5)
C1	0.3961(4)	0.6661(3)	0.04041(13)	0.0178(5)
C2	0.6232(4)	0.6844(3)	0.06039(13)	0.0182(5)
C4	0.4705(4)	0.5058(3)	0.13722(14)	0.0222(5)
C3	0.6674(4)	0.5853(3)	0.12060(14)	0.0206(5)
C10	0.1800(4)	0.8855(3)	0.17886(14)	0.0223(5)
C11	0.2683(4)	0.7527(3)	-0.01594(13)	0.0187(5)
C8	0.5406(4)	0.9200(3)	0.21614(13)	0.0208(5)
C9	0.3451(4)	0.8350(4)	0.22973(13)	0.0214(5)
C5	0.3017(4)	0.5548(3)	0.08797(14)	0.0206(5)
C7	0.4962(4)	1.0211(3)	0.15559(13)	0.0192(5)
C6	0.2727(4)	0.9990(3)	0.13263(13)	0.0192(5)
H2A	0.7302	0.7549	0.0368	0.022
H4A	0.4535	0.4299	0.1774	0.027
H3A	0.8115	0.5753	0.1473	0.025
H10A	0.0258	0.8446	0.1754	0.027
H8A	0.6838	0.9100	0.2434	0.025
H9A	0.3265	0.7536	0.2682	0.026
H5A	0.1462	0.5178	0.0865	0.025
H6A	0.1952	1.0541	0.0917	0.023

APPENDIX 4.

Crystal data and structure refinement for $[Ag_{74}S_{19}(dppp)_6(fc(C\{O\}OCH_2CH_2S)_2)_{18}]$ (**9**)

Empirical formula	C450 H444 Ag74 Fe18 O72 P12 S55
Formula weight	18126.67
Temperature	110(2) K
Wavelength	0.68877 Å
Crystal system	Rhombohedral
Space group	$R\bar{3}$
Unit cell dimensions	a = 36.775(19) Å a= 90°.
	b = 36.775(19) Å b= 90°.
	c = 41.225(19) Å g = 120°.
Volume	48283(42) Å^3
Z	3
Density (calculated)	1.870 Mg/m^3
Absorption coefficient	2.840 mm^{-1}
F(000)	26178
Crystal size	0.04 x 0.07 x 0.07 mm^3
Theta range for data collection	0.78 to 21.02°.
Index ranges	-38<=h<=38, -38<=k<=30, -37<=l<=42
Reflections collected	47737
Independent reflections	12659 [R(int) = 0.0889]
Completeness to theta = 21.02°	99.5 %
Refinement method	Full-matrix least-squares on F^2
Data / restraints / parameters	12659 / 139* / 590
Goodness-of-fit on F^2	1.039
Final R indices [I>2sigma(I)]	R1 = 0.0916, wR2 = 0.2639
R indices (all data)	R1 = 0.1481, wR2 = 0.3076
Largest diff. peak and hole	2.523 and -1.318 e.Å^{-3}

*Disordered ferrocenyl ligand (Fe1/Fe1A) was restrained with SADI/FLAT commands of SHELX (50:50 occupancy)

Atomic coordinates (x 10^4) and equivalent isotropic displacement parameters ($Å^2$ x 10^3) for **9**. U(eq) is defined as one third of the trace of the orthogonalized U^{ij} tensor.

	x	y	z	U(eq)
Ag(1)	3964(1)	5701(1)	2655(1)	90(1)
Ag(2)	4173(1)	5414(1)	1203(1)	90(1)
Ag(3)	4892(1)	6111(1)	1693(1)	83(1)
Ag(4)	3192(1)	5290(1)	434(1)	84(1)
Ag(5)	3812(1)	6261(1)	824(1)	69(1)
Ag(6)	3215(1)	6131(1)	290(1)	76(1)
Ag(7)	3333	6667	2334(1)	74(1)
Ag(8)	4266(1)	6081(1)	270(1)	75(1)
Ag(9)	3072(1)	5173(1)	2158(1)	72(1)
Ag(10)	3426(1)	6046(1)	1896(1)	75(1)
Ag(11)	3220(1)	4727(1)	945(1)	72(1)
Ag(12)	3956(1)	5429(1)	1894(1)	77(1)
Ag(13)	3318(1)	5514(1)	1233(1)	68(1)
Fe(1)	4275(2)	3786(2)	3098(2)	96(3)
Fe(1A)	4260(3)	3729(3)	2958(3)	86(4)
Fe(2)	6755(1)	6059(2)	1156(1)	110(2)
Fe(3)	2938(2)	5509(2)	-1610(1)	122(2)
S(1)	4572(2)	5778(2)	2271(2)	68(2)
S(2)	3255(2)	5052(2)	2683(2)	70(2)
S(3)	4899(2)	5615(2)	1295(2)	88(2)
S(4)	5431(2)	6889(2)	1767(2)	70(2)
S(5)	3909(2)	6469(2)	37(2)	76(2)
S(6)	2569(2)	4804(2)	160(2)	86(2)
S(7)	3783(2)	5575(2)	788(2)	67(2)
S(8)	2831(2)	5340(2)	1673(2)	66(2)
S(9)	2883(2)	5857(2)	830(2)	66(2)
S(10)	3333	6667	1667	71(4)
P(1)	3277(2)	4249(2)	564(2)	70(2)
P(2)	4393(2)	5648(2)	-99(2)	69(2)
O(1)	4380(30)	4400(30)	2346(16)	250(40)
O(2)	4468(11)	4774(11)	2816(10)	68(11)

O(3)	3490(12)	4185(11)	3021(10)	75(11)
O(4)	3800(12)	4361(13)	3495(9)	90(11)
O(1A)	4767(14)	4594(14)	2341(10)	112(13)
O(2A)	4468(10)	4758(10)	2666(9)	58(9)
O(3A)	3481(11)	4110(11)	2872(9)	71(11)
O(4A)	3594(16)	4073(17)	3423(12)	116(16)
O(5)	5626(7)	5515(7)	1428(5)	116(7)
O(6)	5851(11)	5080(12)	1536(8)	190(13)
O(7)	3593(7)	6043(8)	-855(6)	119(7)
O(8)	6392(9)	6677(9)	1551(7)	148(9)
O(9)	3493(9)	5359(10)	-894(7)	156(10)
O(10)	6308(10)	6167(10)	1919(8)	168(11)
O(11)	2555(6)	5075(7)	-771(5)	103(6)
O(12)	2579(9)	4560(9)	-1070(6)	143(9)
C(1)	4613(5)	4250(6)	2763(5)	120(20)
C(2)	4807(5)	4370(5)	3097(6)	120(20)
C(3)	4901(5)	4033(7)	3209(6)	130(30)
C(4)	4765(5)	3706(6)	2944(7)	130(30)
C(5)	4587(6)	3841(7)	2669(4)	180(40)
C(6)	3725(6)	3758(7)	3245(7)	101(19)
C(7)	3868(7)	3599(9)	3487(5)	102(19)
C(8)	3882(5)	3255(7)	3362(6)	130(20)
C(9)	3747(5)	3202(5)	3042(6)	170(40)
C(10)	3650(4)	3513(7)	2970(6)	83(16)
C(1A)	4737(5)	4339(5)	2885(6)	69(13)
C(2A)	4618(6)	4298(5)	3192(6)	104(19)
C(3A)	4692(5)	4015(7)	3328(4)	180(40)
C(4A)	4857(4)	3882(7)	3105(6)	74(14)
C(5A)	4885(5)	4082(7)	2831(6)	87(16)
C(6A)	3675(4)	3649(7)	3054(6)	92(18)
C(7A)	3753(4)	3373(6)	3272(5)	103(19)
C(8A)	3910(6)	3144(4)	3071(7)	170(40)
C(9A)	3929(7)	3279(7)	2728(6)	120(20)
C(10A)	3784(5)	3591(8)	2718(5)	105(19)
C(11A)	4664(13)	4574(12)	2603(13)	95(19)
C(12A)	4348(9)	4986(9)	2454(10)	44(10)

C(14A)	3582(11)	3950(20)	3130(20)	110(20)
C(15A)	3470(40)	4480(30)	2961(15)	160(50)
C(11)	4454(15)	4528(18)	2603(16)	260(90)
C(12)	4364(12)	5036(12)	2627(14)	79(16)
C(14)	3685(12)	4122(19)	3275(16)	76(17)
C(15)	3400(20)	4522(16)	3008(10)	70(19)
C(13)	4732(8)	5430(8)	2473(6)	80(7)
C(16)	3255(8)	4546(8)	2663(6)	80(7)
C(17)	6163(11)	5567(11)	1098(8)	109(10)
C(18)	6491(14)	5480(14)	1002(10)	143(14)
C(19)	6676(12)	5737(13)	763(9)	124(12)
C(20)	6529(12)	5989(12)	697(9)	124(12)
C(21)	6208(10)	5881(10)	929(7)	99(9)
C(22)	6838(9)	6422(10)	1534(7)	120(11)
C(23)	6962(10)	6136(9)	1601(7)	182(19)
C(24)	7274(10)	6201(10)	1387(8)	134(13)
C(25)	7342(9)	6527(10)	1189(6)	141(14)
C(26)	7073(9)	6664(8)	1280(7)	126(12)
C(27)	5892(13)	5353(14)	1368(10)	133(13)
C(28)	5338(10)	5373(10)	1701(7)	97(9)
C(29)	4919(9)	5220(9)	1550(7)	90(8)
C(30)	6439(14)	6405(15)	1696(11)	139(14)
C(31)	5995(14)	6613(14)	1772(10)	152(15)
C(32)	5952(8)	6982(8)	1642(6)	73(7)
C(33)	3497(9)	5745(10)	-1371(6)	122(11)
C(34)	3453(9)	6075(9)	-1506(7)	120(11)
C(35)	3402(11)	6012(11)	-1845(8)	185(19)
C(36)	3415(11)	5643(11)	-1921(7)	157(15)
C(37)	3474(11)	5478(9)	-1628(9)	172(17)
C(38)	2468(10)	5076(10)	-1336(7)	94(9)
C(39)	2454(11)	5443(11)	-1346(8)	110(10)
C(40)	2385(11)	5500(11)	-1666(8)	114(11)
C(41)	2385(12)	5194(12)	-1849(9)	123(11)
C(42)	2444(12)	4925(12)	-1642(9)	123(11)
C(43)	3524(15)	5711(16)	-1008(11)	154(15)
C(44)	3603(10)	6018(10)	-499(7)	93(9)

C(45)	3854(9)	6427(9)	-417(6)	79(7)
C(46)	2532(12)	4869(13)	-1037(9)	124(12)
C(47)	2641(11)	4919(11)	-476(8)	110(10)
C(48)	2477(9)	5027(8)	-201(6)	80(7)
C(49)	3654(8)	4110(8)	684(6)	72(7)
C(50)	3615(11)	3718(10)	587(8)	105(10)
C(51)	3914(12)	3619(12)	680(9)	120(11)
C(52)	4253(11)	3908(11)	864(8)	104(10)
C(53)	4328(10)	4295(10)	941(7)	101(9)
C(54)	4009(9)	4398(8)	853(6)	79(7)
C(55)	2784(9)	3751(9)	506(6)	82(8)
C(56)	2543(9)	3669(9)	228(6)	81(8)
C(57)	2134(11)	3288(11)	214(8)	106(10)
C(58)	2024(11)	3049(11)	463(9)	111(10)
C(59)	2231(11)	3120(11)	717(8)	112(10)
C(60)	2650(9)	3501(10)	759(7)	92(8)
C(61)	4543(8)	5874(8)	-498(6)	78(7)
C(62)	4806(9)	6312(9)	-508(6)	81(7)
C(63)	4937(9)	6506(9)	-830(7)	91(8)
C(64)	4784(10)	6259(10)	-1098(7)	99(9)
C(65)	4532(10)	5832(10)	-1106(7)	97(9)
C(66)	4393(9)	5611(9)	-786(7)	87(8)
C(67)	4830(7)	5591(7)	36(5)	62(6)
C(68)	4865(8)	5536(8)	358(6)	69(7)
C(69)	5217(9)	5511(9)	493(7)	89(8)
C(70)	5512(9)	5536(9)	267(6)	82(8)
C(71)	5481(9)	5603(9)	-52(7)	88(8)
C(72)	5102(9)	5610(9)	-182(7)	87(8)
C(73)	3430(8)	4451(8)	160(6)	68(6)
C(74)	3850(8)	4877(8)	166(6)	78(7)
C(75)	3967(8)	5095(8)	-177(6)	79(7)

APPENDIX 5.
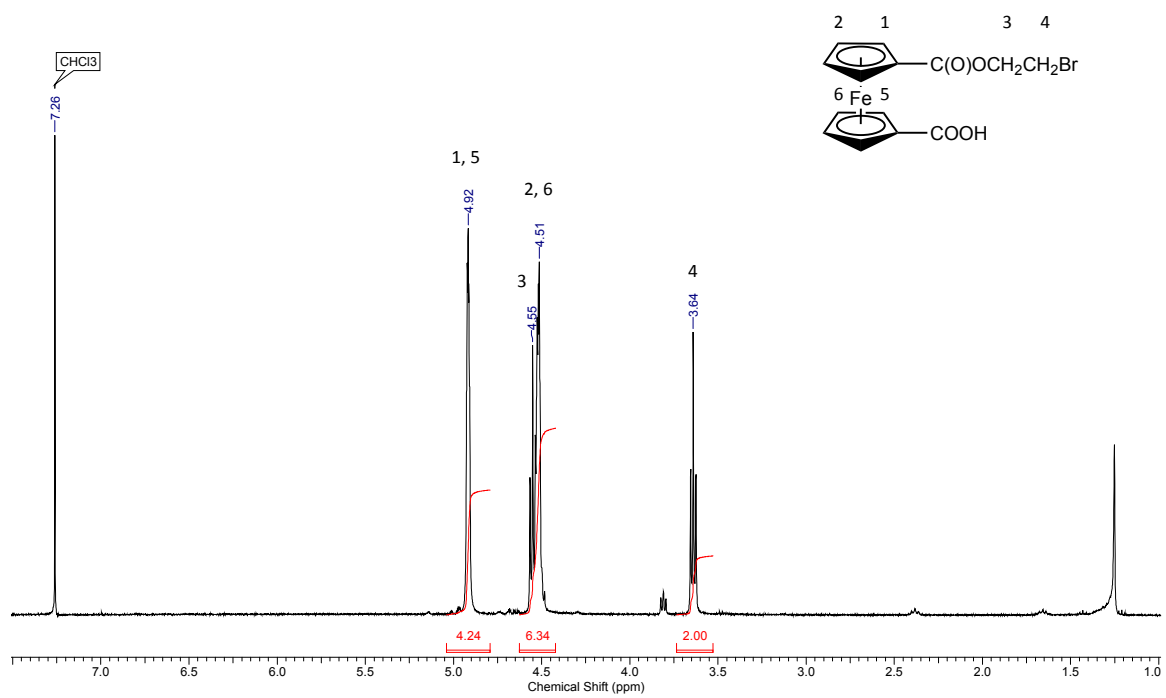
^{1}H NMR spectrum of fc(C{O}OCH$_2$CH$_2$Br)COOH **2**

APPENDIX 6.
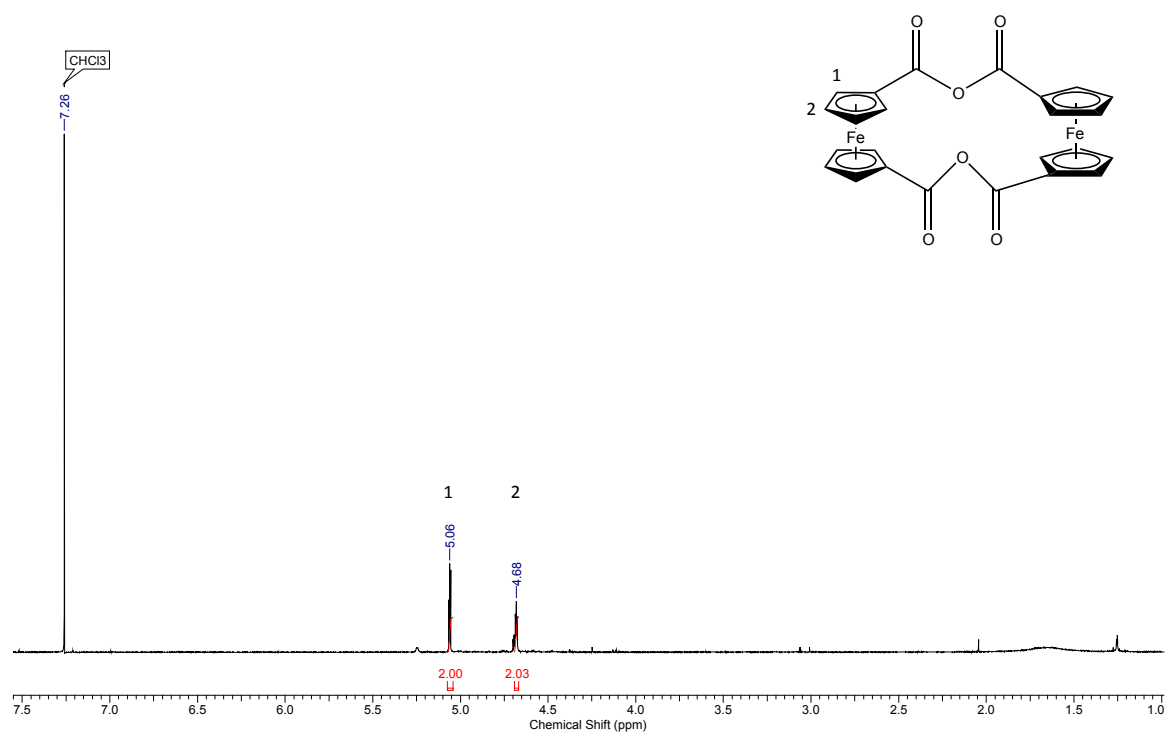
^{1}H NMR spectrum of $(fc(C\{O\}O\{O\}C))_2$ **3**

APPENDIX 7.
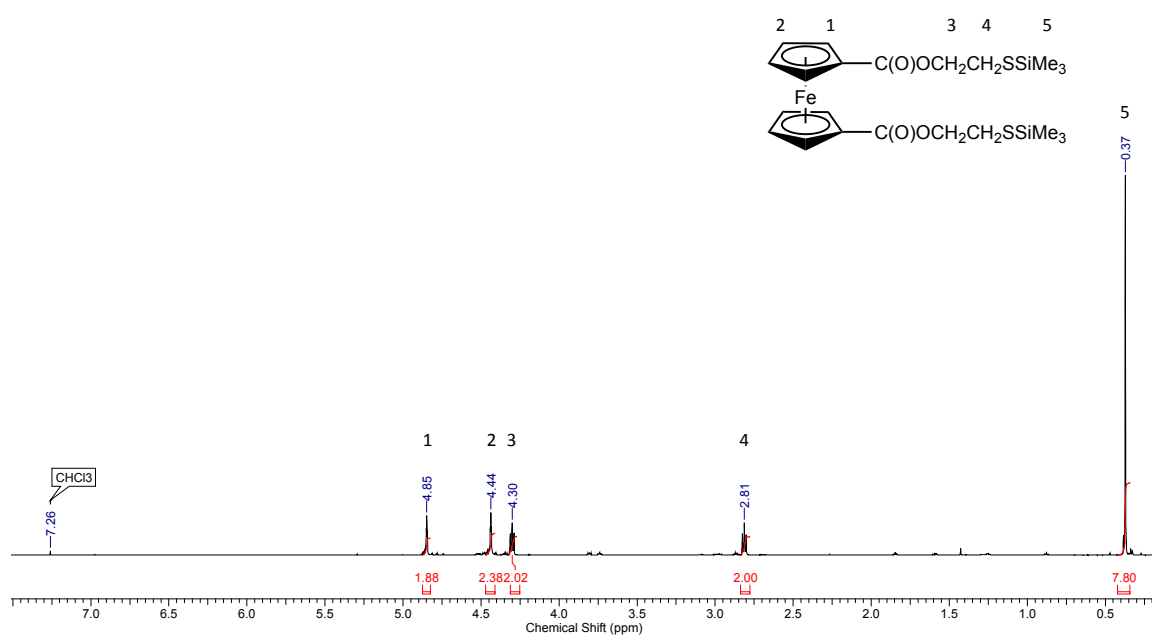
^{1}H NMR spectrum of fc(C{O}OCH$_2$CH$_2$SSiMe$_3$)$_2$ **6**

Curriculum Vitae

Yiyi Liu

Post-Secondary Education and Degree

The University of Western Ontario   London, ON, Canada

M. Sc. Candidate, Department of Chemistry, September 2012 – present.

Shandong University   Jinan, China

Bachelor of Science, National Key Program of Chemistry, June 2012.

Bachelor of Economics, Major in Finance and Banking, June 2012.

Honours and Awards

Graduate Teaching Award Nomination   2013

Teaching Experience

The University of Western Ontario   London, ON, Canada

Teaching Assistant: General Chemistry Labs   2012 – 2014